Rune Steig

Towards Energy Synchronization of Two-Level Voltage Source Converters

A PI Passivity viewpoint on PLL design

Master's thesis in Energy and Environmental Engineering
Supervisor: Gilbert Bergna-Diaz
June 2020

Master's thesis

NTNU
Norwegian University of Science and Technology
Faculty of Information Technology and Electrical Engineering
Department of Electric Power Engineering

NTNU
Norwegian University of Science and Technology

Rune Steig

Towards Energy Synchronization of Two-Level Voltage Source Converters

A PI Passivity viewpoint on PLL design

Master's thesis in Energy and Environmental Engineering
Supervisor: Gilbert Bergna-Diaz
June 2020

Norwegian University of Science and Technology
Faculty of Information Technology and Electrical Engineering
Department of Electric Power Engineering

NTNU
Norwegian University of
Science and Technology

Preface

This master thesis contains the final work as a master student at the Faculty of Information Technology, Mathematics and Electrical Engineering at the Norwegian University of Science and Technology. The master thesis is written in collaboration with SINTEF Energy Research.
From when I started my studies in August 2015, the desire to constant challenge myself has increased throughout the years. The master thesis is not an exception. The thesis concerns topics that I had shortcomings in, whereas my knowledge around the topics has gradually increased. Power electronics is a topic I find really interesting, due to its applicability, especially due to its importance in the integration of more renewable energy sources.
The thesis builds on the specialization project [1] delivered in December 2019, but is not a prerequisite for reading the thesis.

Several persons have contributed academically, practically and with support to this master thesis. I would, therefore, firstly like to thank my main supervisor Gilbert Bergna-Diaz for the countless hours of supervision and always being available. Raymundo Torres-Olguin and Santiago Sanchez-Acevedo, my co-supervisors from SINTEF Energy, do also deserve to be mentioned. Finally, I will like to thank my fellow students for making the study joyful and family, friends and girlfriend for the never-ending support.

Abstract

Substituting traditional fossil energy sources with renewable energy sources will require the use of power electronic converters to interface them to the grid, such as the well-known Voltage Source Converter (VSC). This master thesis investigates the possibility to improve the Phase Locked Loops (PLLs) that are currently used in the industry for grid synchronization of VSCs and are a central part of their control strategy.

From a stability viewpoint, the PLLs used today seem to be designed for synchronizing converters with strong ac grids, where the frequency can be considered constant and the grid is practically unaffected by disturbances. However, this standard solution has a below par performance when synchronizing with weak grids, making the system more prone to undesired unstable behavior. In order to mitigate this risk, small-signal stability studies are usually carried out on a case-by-case basis in order to find an appropriate control tuning that renders the system stable. However, as small-signal methods are based on linearization around a nominal operating point, the system inherent nonlinearities are neglected in the design, consequently making the VSC and the rest of the system vulnerable under larger disturbances. Hence, a more robust PLL that takes the nonlinearities of the system into account has to be designed.

In the specialization project [1], which served as the preliminary groundwork of this master thesis, three challenges associated to the synchronization of the nonlinear model of the VSC and its PLL design were reported; i.e., two related to two different types of system nonlinearities (one trigonometric and a bilinear product), and one related to the unavailability of a state-variable. The work of this master thesis aims to solve two of these three challenges. More precisely, one of the nonlinearities (of trigonometric nature) has been neglected in the model, and consequently in the control design process, to reduce the complexity of the task. Under this approximation, three alternative PLLs have been designed by means of Lyapunov and passivity theories–in order to take into account the remaining system nonlinearity–and compared with a standard PLL used in industry today. In order to design the PLLs, the nonlinear model of the VSC in state-space representation has been validated. It is worth mentioning that in this modeling phase, the angular frequency provided by the PLL, ω_{PLL}, is treated as a *control variable* and hence it is different from the angular frequency of the grid, ω_{g}. This results in two different angular frequencies of the grid; therefore two different Park matrices have to be used in order to represent the system in the two associated synchronous reference frames. The choice regarding which of the two rotating reference frames is associated to the different state variables is what mainly set appart the three alternative PLLs designed.

The passivity-based PLLs showed comparable performance with the traditional PLL, but come with the added advantage of a nonlinear stability certificate. Given that in the design process a simplified model was used, the stability of the different PLLs have also

been analysed via time-domain simulations. Finally, the most promising PLL alternative out of the three has been identified and further modified to be able to operate without the unavailable state measurement and without compromising the stability proof. The performance results related to this PLL are very promising. However, due to lack of time and resources more simulations and test have to be conducted in order to make available this new alternative PLL to the industry. Preferably simulations with a more complex system, where the PLLs face more challenging tasks have to be made, and an extension of the proof to include the neglected trigonometric nonlinearity.

Sammendrag

Denne masteroppgaven ser på muligheten til å forbedre den faselåste sløyfen (PLL) som blir brukt i industrien i dag. PLLen er en del av kontrollsystemet i en frekvensomformer (VSC) og blir brukt til å synkronisere to frekvenser. En VSC er en kraftelektronisk komponent som omformer likestrøm til vekselstrøm og omvendt for å sikre en sikker flyt av energi.

På grunn av det grønne skiftet er det en stadig økning av fornybare energikilder i kraftnettet. En utfordring med dette er at de store sykrongeneratorene i kullkraftverkene forsvinner. Dette skiftet gjør at det totale treghetsmomentet i kraftnettet reduseres, noe som gjør at kravene til de kraftelektroniske komponentene øker.

I spesialiseringsoppgaven [1] ble det oppdaget tre utfordringer knytett til den tradisjonelle PLLen. To av disse tre utforningene har blitt forsøkt løst i denne masteroppgaven. Hovedmålet med dette arbeidet er å løse problemene knyttet til ulinearieter i systemet. Dagens PLLer er designet for et linært system, mens systemene de blir anvendt i er mer komplekse. Tre PLLer som tar ulinearitetene til betrakting har blitt designet ved hjelp av Lyapunov teori samt passivitet teori. I dette arbeidet har den angulære frekvensen som PLLen genererer blitt sett på som en kontrollobjekt. Dette gjør at det trengs to forskjellige angulære frekvenser for å beskrive systemet istedenfor en. En frekvens relatert til nettet, mens den andre er relatert til PLLen. Forskjellen mellom de tre forskjellige PLLene designet i denne oppgaven er i utgangspunktet relatert til hvilken angulær frekvens de ulike tilstandene i systemet er referert til.

De tre ulike PLLene designet er sammenlignet med en simpel PLL som blir brukt i industrien i dag. De blir sammenlignet med hensyn til atferden de får når en referanseverdi er endret, i tillegg stabiliteten de viser. På grunn av differanse mellom stabilitetsresultatene og simuleringsresultatene har simuleringsresultatene blitt favorisert på bakgrunn av at det er en mer kompleks representasjon av systemet sammenlignet med likningene brukt i stabilitetsutregningene.

I tillegg til dette ble den ene PLLen utviklet også til å kanskje ha en løsning på et av de to andre problemene PLLene har i dag. På grunn av dårlig tid ble dessverre ikke mange nok simulering utført, men uansett viser PLLene gode resultater. Dersom flere og mer krevende simuleringer utføres på de ulike PLLene, kan de i beste fall bli en del av industrien. De ulike PLLene designet i dette arbeidet kommer med et stabilitets-sertifikat siden de oppfyller kravene som trengs for at et system skal være globalt asymptisk stabilt.

Table of Contents

List of Tables

List of Figures

Abbreviations

DER	=	Distributed Energy Resources
PLL	=	Phase Locked Loop
PWM	=	Pulse Width Modulation
SRF	=	Synchronous Reference Frame
VSC	=	Voltage Source Converter
VSI	=	Voltage Source Inverter

Chapter 1

Introduction

1.1 Background

The energy demand in the world is increasing and as much as 13 % of the world's population do not have access to electricity [2]. The Paris Agreement aim to strengthen the global response to the threat of climate changes. Hence, the aim is to keep the global temperature 2 degrees Celsius above pre-industrial levels, in addition to pursue efforts to keep the temperature increase to 1.5 degree Celsius [3]. This generation faces a great challenge to increase the standard of living while dealing with the climate challenges. The fulfillment of the goals of the Paris Agreement depends on the development of new technology in addition to decelerate the constant increasing energy consumption.

The transition from traditional fossil energy sources to renewable energy sources is also of paramount importance if the goals set in the Paris Agreement are to be reached. In order to reach the 2-degree Celsius goal the share of electricity produced from renewable energy would need to rise from 14% in 2015 to 63% in 2050 [4]. Renewable energy sources such as solar and wind are usually classified as non-dispatchable distribution units because of their intermittent characteristics and high volatility. Consequently, they are often paired with different energy storage units to provide adequate power to critical loads. However, many distributed energy resources (DER) cannot be connected directly to the grid and must be integrated by use of power electronic converters, such as the two-level voltage source converter (VSC) [5][6]. Power electronic converters such as the ones mentioned above are important enabling technologies in the evolution of the energy grid [7].

A consequence of substituting traditional generation units with renewable energy sources is lower inertia in the grid [8]. Hence, the energy grid is more vulnerable to faults and frequency variations. A VSC is commonly used in providing bidirectional power flow in addition to frequency and voltage decoupling between the utility and the grid [9].

In order to interface different DER, an ac/dc power converter such as the VSC has to synchronize to the frequency of the grid. Today, the most developed synchronization

methods are relying on a Phase Locked Loop (PLL). Although PLLs have been used in many applications for many years, they still have some open challenges which are briefly discussed in [10].

This master thesis continues the work done in the specialization project [1], where the operation principle of a VSC and a PLL were investigated. Hence, basic models including a VSC and different PLLs were tested and compared for both a stiff grid case and a weak grid case. This thesis will, however, be different in the extent that the scope of the project is to design an improved PLL from a stability viewpoint. From the specialization project, three different challenges were identified from the nonlinear synchronization model of the VSC, which need to be considered in the design of an improved PLL. These challenges are listed below.

- *Trigonometric non-linearity:* This nonlinearity appears since two different Park transformations at two different frequencies become necessary to describe the VSC synchronization dynamics; one associated with the frequency of the grid ω_{g}, while the other one associated with the frequency estimated by the PLL, ω_{PLL}.
- *Bilinear products nonlinearity:* This nonlinearity appears naturally when the estimated frequency ω_{PLL} is considered as a control variable instead of a constant. Thus, the cross-coupling terms in the VSC model will consist on a control variable multiplying a state variable.
- *Angle difference state unavailability:* A third problem related to the synchronization model of VSC is that the angle difference state variable $\delta \triangleq \theta_{\mathrm{PLL}} - \omega_{\mathrm{g}} t$ cannot be measured in the weak grid case, and therefore is unavailable for use in the control. This angle is indeed the difference between the two angles used in both Park transformations.

1.2 Objectives

In this master thesis, the main objective is to:

Further investigate the challenges of the nonlinear synchronization model of VSCs connected to weak grids and synthesize an alternative PLL with large signal stability guarantees able to cope with (most of) them.

To achieve the main objective, specific objectives have been set and are listed below.

- Represent and validate the system using the Port-Hamiltonian formalism, to highlight the role of the energy in the system dynamics and use it as a starting point for the control design. Due to the fact that the angular frequency provided by the PLL is treated as a control parameter the port-Hamiltonian representation for switched power converters from [11] will be used.
- Design different PLLs with large signal guarantees by directly applying the PI-Passivity-based Control result from [11], which has proven effective at stabilizing systems with *bilinear products nonlinearities*; i.e., the second challenge listed above.

- Simulate and compare the different PLL alternatives with respect to stability and performance.
- Select the most promising PLL alternative and further modify it to try to solve one of the other remaining two challenges. Given that the challenge related to the *trigonometric nonlinearity* was considered the most challenging, the focus was then directed at solving the third challenge, related to the *angle difference state unavailability*.
- If time allows, the most promising PLL will be tested in the National Smart-Grid Laboratory.
- Evaluate the process and lay the foundation for further work on this area.

1.3 Limitation of Scope

Due to the complexity of the work, it is necessary to limit the scope in order to be able to solve the problems. The limitations made in this work are listed below.

- It is worth mentioning that when designing the alternative PLLs, the focus will be entirely on their structure and not on their tuning. This means that the tuning of the different control parameters of the PLLs is not emphasized in this work. Indeed, this carries as consequence the possibility of poor dynamical performances of the control system, even if stability is achieved. However, this lack of optimal tuning is present in all the PLLs compared, resulting in a fairer comparison between them.
- In order to reduce the number of states describing the system, the system is treated as balanced. This yields only the d and q component of the SRF instead of d,q and 0.
- Additionally, a constant dc-source is considered to be connected to the dc-terminals of the converter, which also reduces the number of states, and eliminates an additional nonlinear challenge related a potential dc capacitor voltage state and duty-cycles.
- The control design in this master thesis is heavily based on the control result of [11], which is successful in stabilizing power electronic dynamics with *bilinear product nonlinearities*. However, this result requires to neglect the *trigonometric nonlinearity* which is present in the synchronization model of VSCs, and is one of the main limitations of this thesis.

1.4 Report Outline

In order to cover the objectives, the thesis is divided into six chapters. The first chapter presents the introduction which includes the background, objectives and limitation of scope.

In Chapter 2, the description of the system is presented as well as general information regarding the most important components of this work. Chapter 2 also introduces how the systems are affected by what angular frequency the different states are related to. The design of the different PLLs are illustrated in Chapter 3, in addition to the necessary theoretical background regarding the design. The procedure of the design is also applied on a known system in order to compare the results. Further, Chapter 4 and Chapter 5 presents the performance results in addition to the theoretical approach on the stability results. Chapter 4 is related to solving the challenge related to the *bilinear product nonlinearity*, while Chapter 5 consists to solving the challenge related to *angle difference state unavailability*. Finally, Chapter 6 including the conclusion and further work is suggested based of the findings in the work.

Chapter 2

Modeling of 2L-VSC for synchronization

In order to design the different alternative PLLs, the first step is to obtain an appropriate model using state-space representation, starting from first principles. The transformation from the natural abc-reference frame to two dq synchronous reference frames –associated to the real and estimated frequencies– is presented in this chapter. Furthermore, the resulting dynamical system will be expressed using the port-Hamiltonian representation, as this is key to apply the control result of [11]. Furthermore, general information about the system's components are also presented in this chapter.

2.1 System Representation

The system of interest in this project is illustrated in Figure 2.1. The dc-source on the dc side of the VSC, V_{dc}, is assumed constant for simplicity. In reality, the dc-source can represent a battery or the dc link in a back-to-back converter. The standard approach for controlling VSC is based on current control loops in the dq SRF, working together with a PLL. The output of the current controller is then modulated with a PWM which is later provided to the VSC. The VSC generates a three-phase voltage e_{abc}, as sketched in Figure 2.1. Part of the LCL-filter is used to emulate the weak grid interface, where L_g and R_g are respectively representing the weak grid Thevenin equivalent inductance and the resistance. Since the thesis is a cooperation between NTNU and SINTEF energy, it is convenient to use somewhat the same values on the parameters they use in their common National Smart Grid Laboratory. The parameters used in this work is listen in Table (2.1).

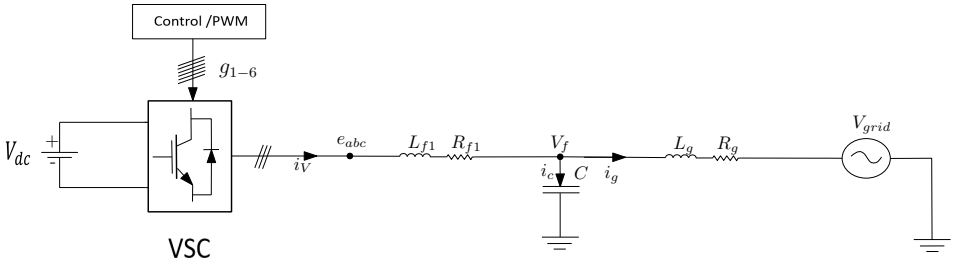

Figure 2.1: The system analysed.

Table 2.1: The parameter values used for the simulations in this work.

	Value	Unit
V_{dc}	700	V
V_{ac}	400	V
f	50	Hz
L_f	3.82	mH
L_g	300	μH
R_f	0.05	Ω
R_g	0.05	Ω
C	60	ηF
f_{sw}	10	kHz
f_{samp}	10	kHz
K_p CC	350	[-]
K_i CC	45 500	[-]
K_pPLL	180	[-]
K_iPLL	1437	[-]
τ	1	[-]

The state-space model of the 2L-VSC in the stationary reference frame with abc coordinates is given in Eq. (2.1) - Eq. (2.3) and is easily found by applying Kirchhoff's laws on the system illustrated in Figure 2.1

The different parameters in the equations are illustrated in Figure 2.1, and the values are listed in Table 2.1.

$$L_f \frac{\mathrm{d}}{\mathrm{d}t} \begin{bmatrix} i_{v,a} \\ i_{V,b} \\ i_{v,c} \end{bmatrix} = \begin{bmatrix} e_a \\ e_b \\ e_c \end{bmatrix} - R_f \begin{bmatrix} i_{v,a} \\ i_{v,b} \\ i_{v,c} \end{bmatrix} - \begin{bmatrix} V_a^0 \\ V_b^0 \\ V_c^0 \end{bmatrix} \tag{2.1}$$

$$C \frac{\mathrm{d}}{\mathrm{d}t} \begin{bmatrix} V_a^0 \\ V_b^0 \\ V_c^0 \end{bmatrix} = \begin{bmatrix} i_{V,a} \\ i_{V,b} \\ i_{V,c} \end{bmatrix} - \begin{bmatrix} i_{g,a} \\ i_{g,b} \\ i_{g,c} \end{bmatrix} \tag{2.2}$$

$$L_g \frac{\mathrm{d}}{\mathrm{d}t} \begin{bmatrix} i_{g,a} \\ i_{g,b} \\ i_{g,c} \end{bmatrix} = \begin{bmatrix} V_a^0 \\ V_b^0 \\ V_c^0 \end{bmatrix} - R_g \begin{bmatrix} i_{g,a} \\ i_{g,b} \\ i_{g,c} \end{bmatrix} - \begin{bmatrix} V_{g,a} \\ V_{g,b} \\ V_{g,c} \end{bmatrix} \tag{2.3}$$

2.1.1 Current Controller

The design of the current controller is not the main focus of this work. However, the basic PLL developed in the specialization project [1] is illustrated in Figure 2.2. Using the cross-coupling PI controllers and feed-forward the system is reduced from a 2×2 MIMO system into two linear SISO- systems. The current controller controls the voltage e_{abc} and hence the current i_v. The outputs of the current controller, m_d and m_q, are later transformed back into the stationary reference frame in order to generate the PWM signals.
In order to focus on the grid synchronization, a power controller is not included in the control system. Implying that the reference currents in the current controller have to be set manually. The current controller used in this work, however, does not include the feed-forward and cross-coupling terms because of the result in Chapter 3.2.3.

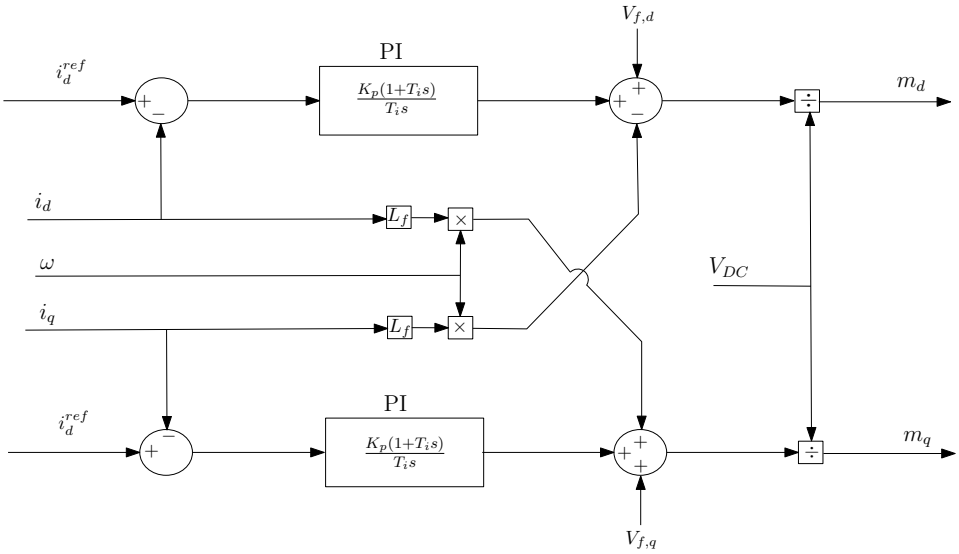

Figure 2.2: The basic current controller designed in the specialization project [1].

2.2 PLL

Grid synchronization is a vital part of the control system of a voltage source converter, and PLLs are often used for this purpose [12]. PLLs are used for grid synchronization, and three alternative PLLs are designed in this work.

The basic structure of a PLL often consists of a phase detector, a low-pass filter, a variable- frequency oscillator and feedback [13]. The PLLs used in this work are working

in the synchronous reference frame, which means that the three-phase voltage is decomposed into two DC signals through a park transformation. This has several advantages, and one of them is the convenient use of PI controllers in the current controller.

As described in [1], the PLL estimates the grid frequency and synchronizes the modulation frequency with the frequency of the grid. Figure 2.3 illustrates the working principle of the PLL. If the voltage vector, V, is aligned with the d-axis, the q-component of the voltage equals zero. The PLL estimates the frequency of the grid and by use of the internal feedback, the modulation frequency is approaching the grid frequency. If the voltage vector, V, is higher than the d-axis component the angular frequency is decreased and on the contrary, if the voltage vector is lower than the d-axis the angular frequency is increasing. This repeats until the voltage vector equals the d-axis component.

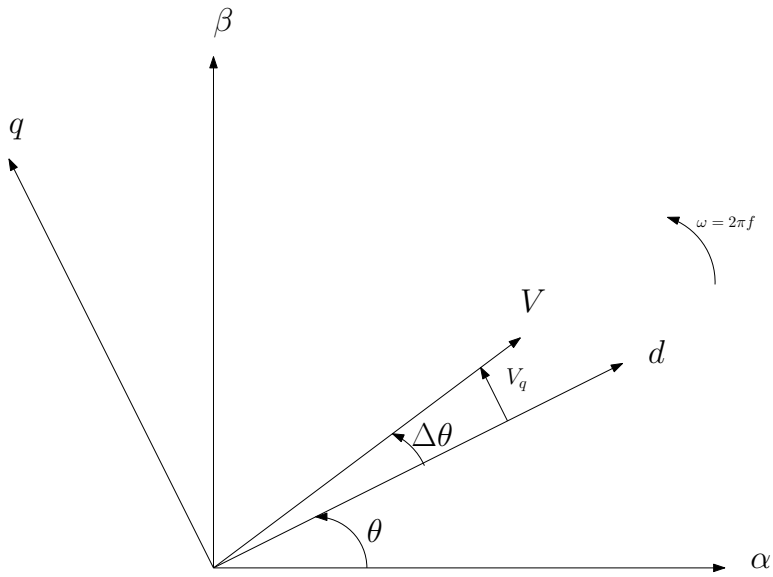

Figure 2.3: An illustration of the working principle of a phase-locked loop (PLL).

When the q-axis component equals zero the active and reactive power flow can be controlled linearly with respect to I_d and I_q. The active and reactive power relationship is illustrated in Eq. 2.4 and Eq. 2.5. Thus, if $V_q = 0$, the active power can be controlled with I_d and reactive power can be controlled with I_q.

$$P = \begin{bmatrix} V_d \\ V_q \end{bmatrix} \begin{bmatrix} 1 & 0 \\ 0 & 1 \end{bmatrix} \begin{bmatrix} i_d \\ i_q \end{bmatrix} \tag{2.4}$$

$$Q = \begin{bmatrix} V_d \\ V_q \end{bmatrix} \begin{bmatrix} 0 & -1 \\ 1 & 0 \end{bmatrix} \begin{bmatrix} i_d \\ i_q \end{bmatrix} \tag{2.5}$$

The structure of on of the standard PLL used in this thesis as a reference for comparison is shown in Figure 2.4[14]. The angle difference δ is estimated as the arc tangent of the

relationship between V_q and V_d. To gain more control of the PLL, a parameter τ is included in the feedback loop. Hence, the contribution from the δ term can be controlled by tuning τ. For the three alternative PLLs designed in this work, the additional terms are included in the summation before the PI controller. For the basic PLL this summation has no practical effect but is advantageous for illustration.

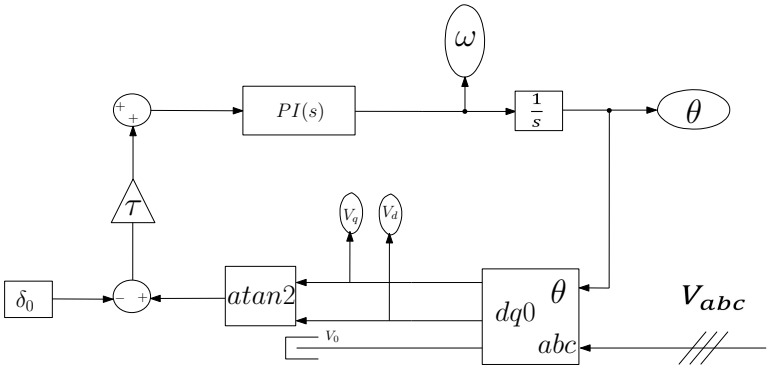

Figure 2.4: The base PLL for this project.

Where δ_0 is the calculated steady state value of δ. For a strong grid case, δ is correctly the arctangent relationship between V_q and V_d and is available for measurement. Nevertheless, for a weak grid case, the relationship is only an approximation, and therefore δ is unavailable. This is further elaborated in the next section.

2.3 Park Transformation

In this work, PI-controllers have been used in the current controller, and therefore, Park transformations are required to transform the voltage and current signals from their natural abc coordinates into the synchronous reference frame dq coordinates. This allows for treating the resulting signals as dc-signals. More precisely, the Park transformation first transforms a three-phase signal shifted 120 degrees into a two-phased signal shifted 90 degrees, and after that make the reference signal rotate with the same speed as the two signals, providing two constant signals.

The matrices used in order to conduct the park transformation are illustrated in Eq. (2.6) for a generic variable x, and its inverse in Eq. (2.7), which is used to transform from SRF to the stationary reference frame.

$$\begin{bmatrix} x_d \\ x_q \\ x_0 \end{bmatrix} = 2/3 \begin{bmatrix} \cos(\theta) & \cos(\theta - \frac{2\pi}{3}) & \cos(\theta + \frac{2\pi}{3}) \\ -\sin(\theta) & -\sin(\theta - \frac{2\pi}{3}) & -\sin(\theta + \frac{2\pi}{3}) \\ \frac{1}{2} & \frac{1}{2} & \frac{1}{2} \end{bmatrix} \begin{bmatrix} x_a \\ x_b \\ x_c \end{bmatrix} \tag{2.6}$$

$$\begin{bmatrix} x_a \\ x_b \\ x_c \end{bmatrix} = \begin{bmatrix} \cos(\theta) & -\sin(\theta) & 1 \\ \cos(\theta - \frac{2\pi}{3}) & -\sin(\theta - \frac{2\pi}{3}) & 1 \\ \cos(\theta + \frac{2\pi}{3}) & -\sin(\theta + \frac{2\pi}{3}) & 1 \end{bmatrix} \begin{bmatrix} x_d \\ x_q \\ x_0 \end{bmatrix} \tag{2.7}$$

It is worth mentioning that two different frequencies are used to describe the system in order to capture the synchronization mechanism an allow for a reformulation of the PLL design. One is related to the (a priori unavailable) angle of the grid $\omega_{\text{g}}t$, and the other one is related to angle θ_{PLL} estimated by the PLL, which in turn is associated to the estimated frequency ω_{PLL}. Often, the system is modelled with only one frequency, which implies the assumption that the PLL is able to provide the grid frequency at all times, thus ignoring the synchronization dynamics.

As a consequence of having two different frequencies describing different states in the system is that one state variable appearing in the differential equation describing the dynamics of a second state may be using different Park transformations, and hence referred to different SRFs. This results in a multiplication of the different Park matrices yielding the relationship expressed in Eq. (2.8) and Eq. (2.9), with

$$\delta = \theta_{pll} - \omega_g t.$$

This relationship was also reported in the specialization project [1] and is one of the three challenges related to the PLL, as it represents a *trigonometric nonlinearity*.

$$T(\delta) = P_{\theta_{\text{pll}}} \cdot P^{-1}_{\omega_{\text{g}}t} = \begin{bmatrix} \cos(\delta) & -\sin(\delta) \\ \sin(\delta) & \cos(\delta) \end{bmatrix} \tag{2.8}$$

$$T^{\top}(\delta) = P_{\omega_{\text{g}}t} \cdot P^{-1}_{\theta_{\text{pll}}} = \begin{bmatrix} \cos(\delta) & \sin(\delta) \\ -\sin(\delta) & \cos(\delta) \end{bmatrix} \tag{2.9}$$

In this work, three different PLLs have been designed, and what differs the different PLLs is what frequency the different states are referred to.

2.3.1 Traditional Modeling

In order to better illustrate what differs the synchronization modeling of VSCs from the traditional approach, the traditional model with only one Park transform is also included. In this approach, the angular frequency provided by the PLL, ω_{pll}, is treated as equal to the angular frequency of the grid, ω_{g} at any given time; i.e., $\omega_{\text{g}} = \omega_{\text{pll}}$. As discussed in [1], this consideration is only correct in steady state (if $\dot{\delta} = 0$). Consequently, once the system is out of its steady state, this consideration is no longer strictly correct. Indeed, the larger disturbance affecting the system, the higher the error.

In the synchronous reference frame, the traditional way of describing the system is expressed in Eq. (2.10) - Eq. (2.12). There is a total of six states describing the system, and the system has only one frequency. The PLLs used today are often derived from these equations. For a stiff grid, this interpretation might be sufficient, since the grid is nearly unaffected by disturbances. For a weak grid, however, the frequency of the grid will be influenced by disturbances. Due to the error in the estimation of the grid, the VSC might disconnect because the PLL does not manage to synchronize. As described in [1], the future system will be even "weaker" due to the substitution of coal power plants to renewable energy sources.

$$L_f \frac{\mathrm{d}}{\mathrm{d}t}\begin{bmatrix} i_{v,d} \\ i_{v,q} \end{bmatrix} = \begin{bmatrix} e_d \\ e_q \end{bmatrix} + \begin{bmatrix} -R_f & L_f\omega_{\text{pll}} \\ -L_f\omega_{\text{pll}} & -R_f \end{bmatrix} \begin{bmatrix} i_{v,d} \\ i_{v,q} \end{bmatrix} - \begin{bmatrix} v_{f,d} \\ v_{f,q} \end{bmatrix} \tag{2.10}$$

$$C_f \frac{\mathrm{d}}{\mathrm{d}t}\begin{bmatrix} v_{f,d} \\ v_{f,q} \end{bmatrix} = \begin{bmatrix} 0 & C_f\omega_{\text{pll}} \\ -C_f\omega_{\text{pll}} & 0 \end{bmatrix} \begin{bmatrix} v_{f,d} \\ v_{f,q} \end{bmatrix} + \begin{bmatrix} i_{v,d} \\ i_{v,q} \end{bmatrix} - \begin{bmatrix} i_{g,d} \\ i_{g,q} \end{bmatrix} \tag{2.11}$$

$$L_g \frac{\mathrm{d}}{\mathrm{d}t}\begin{bmatrix} i_{g,d} \\ i_{g,q} \end{bmatrix} = \begin{bmatrix} -R_g & L_g\omega_{\text{pll}} \\ -L_g\omega_{\text{pll}} & -R_g \end{bmatrix} \begin{bmatrix} i_{g,d} \\ i_{g,q} \end{bmatrix} + \begin{bmatrix} v_{f,d} \\ v_{f,q} \end{bmatrix} - \begin{bmatrix} V_{g,d} \\ V_{g,q} \end{bmatrix} \tag{2.12}$$

2.3.2 Alternative Models

As already stated, the system is modeled with two different angular frequencies in this work. As described in Chapter 2.3, this approach requires two Park matrices to describe the system. Hence, the main difference between the different PLLs designed is mainly what Park transformation different states are related to. This selection is sketched in Figure 2.5 for the different PLLs.

In order to separate the different PLLs designed in this work, the PLLs have been named alternative 0, alternative 1 and alternative 2. Initially, the scope of this work is to design one improved PLL, but different alternative formulations have been discovered in the process.

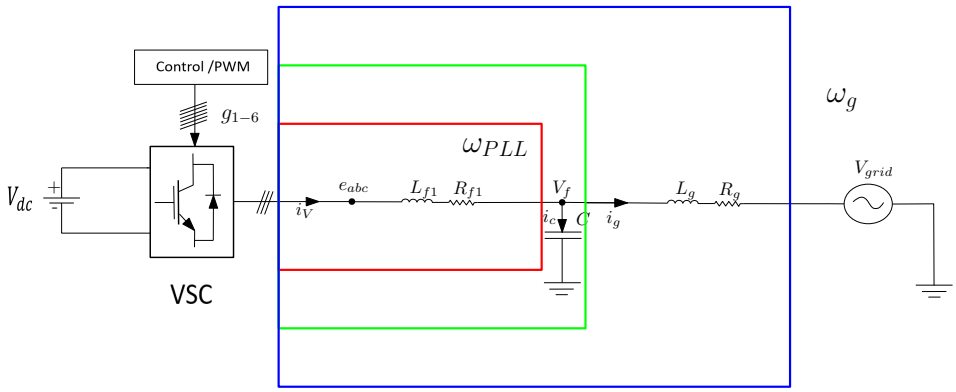

Figure 2.5: Illustration of what angular frequency the different PLLs are related to. Red box = Alternative 0, Green box = Alternative 1 and Blue box = Alternative 2

Figure 2.5 illustrates how the different alternative PLLs referring to the two frequencies. The list below briefly indicates what separates the different PLLs.

- Alternative 0: The only states that are related to ω_{pll} are $i_{v,d}$ and $i_{v,q}$, illustrated with the red box in Figure 2.5. The rest of the states are related to Park transform at ω_{g}.
- Alternative 1: In addition to $i_{v,d}$ and $i_{v,d}$, $v_{f,d}$ and $v_{f,q}$ are also referred to ω_{PLL}, as illustrated with the green box in Figure 2.5. The rest of the states are related to Park transform at ω_{g}.

- Alternative 2: All the states are related to ω_{pll}, including $i_{g,d}$ and $i_{g,q}$. Naturally, the voltage of the grid is still referred to the frequency of the grid. Illustrated with a blue box in Figure 2.5.

As introduced in Chapter 2.3, a *trigonometric nonlinearity* term appears when the system is treated with two different frequencies resulting in different descriptions of the system depending on what PLL has been associated to each variable. In the following sections, the differential equations describing the different systems are given.

Because the two frequencies are time-varying and not equal, one additional state is needed to describe the new systems. The new state equation is expressed in Eq.(2.13).

$$\dot{\delta} = \theta_{\text{pll}} - \omega_{\text{g}} t \tag{2.13}$$

where the derivative of θ_{pll} is ω_{pll}, which is the angular frequency determined by the PLL. The angular frequency of the PLL varies in order to synchronize with the grid. Moreover, key to the results of this master thesis is to view ω_{pll} as a control variable. This results in a system with three control parameters when also taking into account the output voltage of the converter e_d and e_q. For the alternative models, the individual characteristics are marked with the same color codes illustrated in Figure 2.5.

2.3.3 Alternative 0

From Figure 2.5 it can be seen that the only states refereed to ω_{pll} in alternative 0 are $i_{v,d}$ and $i_{v,q}$. This representation was briefly discussed in the specialization project [1]. Hence with only $i_{v,d}$ and $i_{v,q}$ referred to ω_{pll}, the system can be described by Eq. (2.14) - Eq. (2.16).

$$\mathrm{L}_f \frac{\mathrm{d}}{\mathrm{d}t}\begin{bmatrix} i_{v,d} \\ i_{v,q} \end{bmatrix} = \begin{bmatrix} e_d \\ e_q \end{bmatrix} + \begin{bmatrix} -R_f & L_f\omega_{\text{pll}} \\ -L_f\omega_{\text{pll}} & -R_f \end{bmatrix}\begin{bmatrix} i_{v,d} \\ i_{v,q} \end{bmatrix} + \begin{bmatrix} -\cos(\delta) & -\sin(\delta) \\ \sin(\delta) & -\cos(\delta) \end{bmatrix}\begin{bmatrix} v_{f,d} \\ v_{f,q} \end{bmatrix} \tag{2.14}$$

$$C_f \frac{\mathrm{d}}{\mathrm{d}t}\begin{bmatrix} v_{f,d} \\ v_{f,q} \end{bmatrix} = \begin{bmatrix} 0 & C_f\omega_g \\ -C_f\omega_g & 0 \end{bmatrix}\begin{bmatrix} v_{f,d} \\ v_{f,q} \end{bmatrix} + \begin{bmatrix} \cos(\delta) & -\sin(\delta) \\ \sin(\delta) & \cos(\delta) \end{bmatrix}\begin{bmatrix} i_{v,d} \\ i_{v,q} \end{bmatrix} - \begin{bmatrix} i_{g,d} \\ i_{g,q} \end{bmatrix} \tag{2.15}$$

$$L_g \frac{\mathrm{d}}{\mathrm{d}t}\begin{bmatrix} i_{g,d} \\ i_{g,q} \end{bmatrix} = \begin{bmatrix} v_{f,d} \\ v_{f,q} \end{bmatrix} + \begin{bmatrix} -R_g & L_g\omega_g \\ -L_g\omega_g & -R_g \end{bmatrix}\begin{bmatrix} i_{g,d} \\ i_{g,q} \end{bmatrix} - \begin{bmatrix} V_{g,d} \\ V_{g,q} \end{bmatrix} \tag{2.16}$$

$$\frac{\mathrm{d}}{\mathrm{d}t}\delta = \omega_{\text{pll}} - \omega_g \tag{2.17}$$

2.3.4 Alternative 1

For this alternative, $i_{v,d}$, $i_{v,q}$, $v_{f,d}$ and $v_{f,q}$ are referred to ω_{pll}. As a result, the system can be described by Eq. (2.18) - Eq. (2.20). An interesting observation with these equations compared to alternative 0, is that the trigonometric identity matrices have moved from nearby the VSC closer to the grid. Because $v_{f,d}$ and $v_{f,q}$ are referred to ω_{pll}, ω_{pll} does also appear in the voltage dynamics for the system.

$$L_f \frac{\mathrm{d}}{\mathrm{d}t}\begin{bmatrix} i_{v,d} \\ i_{v,q} \end{bmatrix} = \begin{bmatrix} e_d \\ e_q \end{bmatrix} + \begin{bmatrix} -R_f & L_f\omega_{\text{pll}} \\ -L_f\omega_{\text{pll}} & -R_f \end{bmatrix} \begin{bmatrix} i_{v,d} \\ i_{v,q} \end{bmatrix} - \begin{bmatrix} v_{f,d} \\ v_{f,q} \end{bmatrix} \tag{2.18}$$

$$C_f \frac{\mathrm{d}}{\mathrm{d}t}\begin{bmatrix} V_d^0 \\ V_q^0 \end{bmatrix} = \begin{bmatrix} 0 & C_f\omega_{\text{pll}} \\ -C_f\omega_{\text{pll}} & 0 \end{bmatrix} \begin{bmatrix} v_{f,d} \\ v_{f,q} \end{bmatrix} + \begin{bmatrix} i_{v,d} \\ i_{v,q} \end{bmatrix} - \begin{bmatrix} \cos(\delta) & -\sin(\delta) \\ \sin(\delta) & \cos(\delta) \end{bmatrix} \begin{bmatrix} i_{g,d} \\ i_{g,q} \end{bmatrix} \tag{2.19}$$

$$L_g \frac{\mathrm{d}}{\mathrm{d}t}\begin{bmatrix} i_{g,d} \\ i_{g,q} \end{bmatrix} = \begin{bmatrix} -R_g & L_g\omega_g \\ -L_g\omega_g & -R_g \end{bmatrix} \begin{bmatrix} i_{g,d} \\ i_{g,q} \end{bmatrix} + \begin{bmatrix} \cos(\delta) & \sin(\delta) \\ -\sin(\delta) & \cos(\delta) \end{bmatrix} \begin{bmatrix} v_{f,d} \\ v_{f,q} \end{bmatrix} - \begin{bmatrix} V_{g,d} \\ V_{g,q} \end{bmatrix} \tag{2.20}$$

$$\frac{\mathrm{d}}{\mathrm{d}t}\delta = \omega_{\text{pll}} - \omega_g \tag{2.21}$$

2.3.5 Alternative 2

In this representation, all the states are referred to ω_{pll}. Leaving the grid voltage the only term including the trigonometric matrix. The differential equations describing the alternative 2 model are illustrated in Eq. (2.22 - Eq. (2.25). Together with the alternative 1 model, $v_{f,d}$ and $v_{f,q}$ are also here referred to ω_{pll}. Hence, ω_{pll} does also appear in the voltage dynamics for this system. Because all the six states of the system are related to ω_{pll}, the only state where ω_g appears is in the 7$^{\text{th}}$ state of the system.

$$L_f \frac{\mathrm{d}}{\mathrm{d}t}\begin{bmatrix} i_{v,d} \\ i_{v,q} \end{bmatrix} = \begin{bmatrix} e_d \\ e_q \end{bmatrix} + \begin{bmatrix} -R_f & L_f\omega_{\text{pll}} \\ -L_f\omega_{\text{pll}} & -R_f \end{bmatrix} \begin{bmatrix} i_{v,d} \\ i_{v,q} \end{bmatrix} - \begin{bmatrix} v_{f,d} \\ v_{f,q} \end{bmatrix} \tag{2.22}$$

$$C_f \frac{\mathrm{d}}{\mathrm{d}t}\begin{bmatrix} v_{f,d} \\ v_{f,q} \end{bmatrix} = \begin{bmatrix} 0 & C_f\omega_{\text{pll}} \\ -C_f\omega_{\text{pll}} & 0 \end{bmatrix} \begin{bmatrix} v_{f,d} \\ v_{f,q} \end{bmatrix} + \begin{bmatrix} i_{v,d} \\ i_{v,q} \end{bmatrix} - \begin{bmatrix} i_{g,d} \\ i_{g,q} \end{bmatrix} \tag{2.23}$$

$$L_g \frac{\mathrm{d}}{\mathrm{d}t}\begin{bmatrix} i_{g,d} \\ i_{g,q} \end{bmatrix} = \begin{bmatrix} -R_g & L_g\omega_{\text{pll}} \\ -L_g\omega_{\text{pll}} & -R_g \end{bmatrix} \begin{bmatrix} i_{g,d} \\ i_{g,q} \end{bmatrix} + \begin{bmatrix} v_{f,d} \\ v_{f,q} \end{bmatrix} - \begin{bmatrix} \cos(\delta) & \sin(\delta) \\ -\sin(\delta) & \cos(\delta) \end{bmatrix} \begin{bmatrix} V_{g,d} \\ V_{g,q} \end{bmatrix} \tag{2.24}$$

$$\frac{\mathrm{d}}{\mathrm{d}t}\delta = \omega_{\text{pll}} - \omega_g \tag{2.25}$$

2.3.6 On the estimation of a measurable δ

The arctanget estimation of δ is replaced by an exact value of δ, in order to fully focus on the nonlinear challenge. The PLL illustrated in Chapter 2.2, approximate the q-component of the grid to equal zero. Which as discussed earlier, are correct for a weak grid. As shown in Eq. (2.8), trigonometric occurs when using two different Park transformations. This trigonometric term does occur when the grid is referred to another frequency compared to the measured voltages, $V_{f,d}$ and $v_{f,q}$.

The relationship between the measurable grid voltage and the actual grid voltage are described by Eq. 2.26.

$$V_{d,q}^m = \begin{bmatrix} \cos(\delta) & -\sin(\delta) \\ \sin(\delta) & \cos(\delta) \end{bmatrix} \begin{bmatrix} V_d \\ V_q \end{bmatrix} \tag{2.26}$$

Where

$$\delta = \theta_{\text{pll}} - \omega_g t \tag{2.27}$$

Where θ_{pll} is the integrate of ω_{pll}. Hence the derivative of δ is:

$$\dot{\delta} = \omega_{\text{pll}} - \omega_g \tag{2.28}$$

By assuming $V_q = 0$, the following relationship can be found by help of trigonometrics applied on Eq. (2.26):

$$\begin{aligned} V_d^m &= \cos(\delta) V_d \\ V_q^m &= \sin(\delta) V_d \\ \delta &= \arctan\left(\frac{V_q^m}{V_d^m}\right) \end{aligned}$$

This results in the fact that δ can be treated as a measurable parameter, for a stiff grid. Selecting V_q as 0 is necessary to obtain the relationship above, and is equivalent to set the reference phase angle to 0 to V_{abc}, and gives the correct measure of δ. In addition, this PLL is one of the most widely used and therefore is considered the reference for comparison with the alternative PLL proposed in this work.
For a weak grid, on the other hand, δ is not measurable as V_q cannot be set to zero since it is now a state variable. Yielding an additional term in the description of θ, which is not measurable. For a weak grid, Eq. (2.29) describes δ.

$$\delta = \arctan\left(\frac{v_{f,q}^m}{v_{f,d}^m}\right) - \arctan\left(\frac{v_{f,q}}{v_{f,d}}\right) \tag{2.29}$$

Where $v_{f,q}$ and $v_{f,d}$ are the actual voltage, which is not measurable.

This implies that δ can be expressed with both Eq. (2.27) and Eq. (2.29). An essential difference between these two representations is that Eq. (2.27) is varying with time.

In order to first focus on the challenges related to the nonlinearities, most of the simulations are initially conducted under the considerable approximation of having the exact knowledge of δ. Thus, instead of estimating δ with the inverse tangential relationship of $v_{f,q}^m$ and $v_{f,d}^m$, the real δ is found by use of Eq. (2.27) and Eq. (2.28).
Figure 2.6 illustrates how the exact δ is provided in this work.

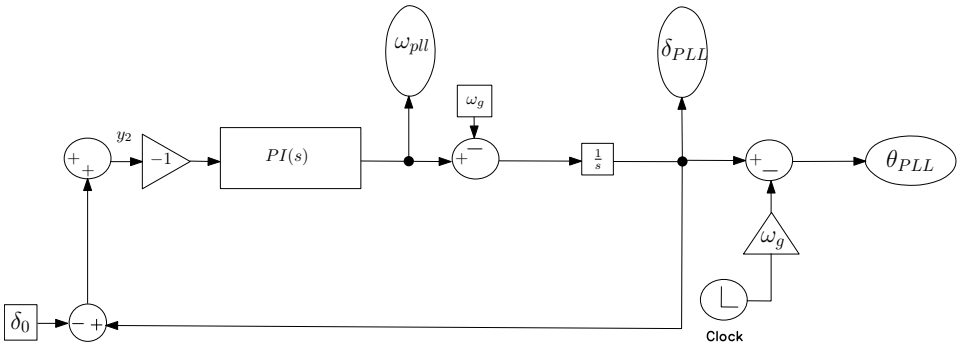

Figure 2.6: Illustration of how the exact δ is provided.

In order to get ω_g time varying, a clock is included in the PLL.

Chapter 3

Energy Shaping for Synchronization

This chapter will focus on the design of the different PLLs. Three alternative PLLs have been designed by means of Lyaponov and passivity theories - in order to take into account the remaining system nonlinearity. The design is heavily based on the control results from [11], which is successful in stabilizing power electronic dynamics with *bilinear product nonlinearities*. Because the angular frequency from the PLL, ω_{pll}, is treated as a control variable in this work, the equations used in [11] are extended.

3.1 Preliminaries in Nonlinear Control

Physical systems inherent nonlinearities that can produce undesirable effects in the operation. As a result of this, control methods and analysis techniques to compensate for and/or take into account the nonlinear effect have been developed. Unlike linear systems, nonlinear systems cannot be analysed in the frequency domain [15]. Hence, theoretical knowledge on nonlinear stability theory is vital in the design of a robust controller in a nonlinear system.

Lyapunov direct and indirect stability methods are used in the design and analysis of a dynamical system. The direct method is related to general energy concepts such that the motion of a system is stable if the system's energy decreases at all times and is able to take into account the system nonlinearity.

3.1.1 Lyapunov Stability

Even though Lyapunov lived for more than a hundred years ago, the mathematician and engineer described how well a system operated around a desired equilibrium point. The Lyapunov theory says that an equilibrium point is stable if all solutions starting at nearby

points stay at nearby points, otherwise, it is unstable. The system can be said to be asymptotically stable if not only the solution stays close by the equilibrium point, but within as time tends towards infinity, the solution tends towards the equilibrium point [16].
In [16], the definition of the equilibrium point $x = 0$ of a system is

- stable if, for each $\epsilon > 0$, there is $\delta = \delta(\epsilon) > 0$ such that

$$\|x(0)\| < \delta \Rightarrow \|x(t))\| < \epsilon,\ \forall t \geq 0$$

- unstable if it is not stable.
- asymptotically stable if it is stable and δ can be chosen such that

$$\|x(0))\| < \delta \Rightarrow \lim_{t\to\infty} x(t) = 0$$

Where the $\epsilon - \delta$ requirement for stability takes a challenge-answer form. For any value of ϵ that the challenger may care to designate, the system must produce a value of δ (possible dependent on ϵ), such that a trajectory starting in a δ close to the origin will never leave the ϵ area.

Lyapunov's stability theorem

let $x = 0$ be the equilibrium point for the system, and $D \subset R^n$ be an domain containing $x = 0$. Let $V : D \to R$ be a continuously differentiable function such that:

$$V(0) = 0 \ \ and \ \ V(x) > 0 \ in \ D - \{0\}$$
$$\dot{V}(x) \leq 0 \ \ in \ \ D$$

Then, x=0 is stable. Moreover, if

$$\dot{V}(x) < 0 \ \ in \ \ D - \{0\}$$

then $x = 0$ is asymptotically stable.

In other words; The system is asymptotically stable if the derivative of the function decreases, except for the value of the equilibrium point. Because in the equilibrium point, the derivative of the function equals zero.

3.1.2 Passivity

Passivity can be viewed as an extension of Lyapunov's theory to systems in open-loop, heavily relying on energy conservation and transformation principles [16] and useful starting point for designing controllers of physical (passive) systems. In [17] the theory is applied to switching power converters. The article proves and illustrates how switching power converters can be stabilized by simple PI controllers applied to the so-called *passive output*. The result in [17] is *equilibrium-independent*. Therefore, it is possible to

globally asymptotically stabilize the system to any desired equilibrium. This is achieved by using the incremental model of the system associated to the incremental state variables

$$\tilde{x} = x - x^{\star}$$

where $x^{\star}$ are the known equilibrium points and x are the respective states.

Passivity theorem [16]

Consider a general state space system $\sum$ which can be described as

$$\dot{x} = f(x,u), \quad x(0) - x_0 \varepsilon \mathbb{R}^n,$$

$$y = h(x,u),$$

Where $x\varepsilon\mathbb{R}^n$ is the state vector, input u $\varepsilon\mathbb{R}^m$ and the output $y = \varepsilon\mathbb{R}^m$

The system $\sum$ is passive if it is dissipative with supply rate $w(u,y) = u^T y$.
It is input strictly passive if it is dissipative with supply rate $w(u,y) = u^T - \delta_i \left\|u\right\|^2$ where $\delta_i > 0$.

The $\sum$ is dissipative with respect to the supply $w(u,y) : \mathbb{R}^m \times \mathbb{R}^m \to \mathbb{R}^n$ if and only if there exists a storage function $H : \mathbb{R}^n \to \mathbb{R}_{\geq 0}$ such that

$$H(x(T)) \leq H(x(0)) + \int_0^T w(u(t)), y(t))\, dt$$

for all, all T ≥ 0 and all $x_0\varepsilon\mathbb{R}^n$

3.1.3 Port- Hamiltonian

In order to analyse the system and design a passivity-based controller, a representation of the system using the port-Hamiltonian formalism becomes convenient. For most nonlinear systems

$$\dot{x} = f(x,u)$$

or even

$$\dot{x} = f(x) + g(x)u$$

can be too general. Hence, the $f(x)$ from the equation above can be further divided in the case of physical systems.

Numerous nonlinear physical systems can be represented by the port-Hamiltonian formalism illustrated in Eq.3.1.

$$\dot{x} = [\mathcal{J}(x) - \mathcal{R}(x)]\nabla\mathcal{H}(x) + g(x)u \tag{3.1}$$

where x is a vector containing the state, $\mathcal{J}(x)$ is the interconnection matrix and $\mathcal{R}(x)$ is the dissipation matrix. $\mathcal{H}(x)$ is the stored energy of the system or the *Hamiltonian* and can be often expressed by:

$$\mathcal{H}(x) = \frac{1}{2} x^\intercal Q x$$

where Q is a symmetric matrix. The diagonal includes 1 divided by the storage units of each differential equation.

$$Q = Q^\intercal > 0$$

The interconnection matrix is a skew-symmetric matrix, hence $\mathcal{J}(x) = -\mathcal{J}^\intercal(x)$. The dissipation matrix, $\mathcal{R}(x)$ also has some characteristics worth noticing. The dissipated energy of the system can never be negative, which means that $\mathcal{R}(x) \geq 0$.

The stored energy of the system derived with respect to time can be expressed as:

$$\dot{\mathcal{H}} = \nabla^\intercal \mathcal{H}(x) \cdot \dot{x} \tag{3.2}$$

with $\nabla = \dfrac{\partial}{\partial x}$.

Combining Eq. (3.1) and Eq. (3.2) gives Eq. (3.3).

$$\dot{\mathcal{H}} = \overbrace{\nabla^\intercal \mathcal{H}(x) \mathcal{J}(x) \nabla \mathcal{H}(x)}^{\text{Power Conservation}} - \overbrace{\nabla^\intercal \mathcal{H}(x) \mathcal{R}(x) \nabla \mathcal{H}(x)}^{\text{Power Dissipation}} + \overbrace{\nabla^\intercal \mathcal{H}(x) g(x)}^{\text{Passive Output} \quad y^\intercal} \cdot u \tag{3.3}$$

Due to the characteristics of the dissipation matrix, and the interconnection matrix the power conservation in Eq. (3.3) will be zero and the power dissipated will be higher or equal zero. This yields the following relationship:

$$\dot{\mathcal{H}} \leq y^\intercal u \tag{3.4}$$

Where $y^\intercal$ is the passive output term of Eq. (3.3). Hence, Eq. (3.4) can be characterized as a passive system. Thus, the system represented by the port-Hamiltonian dynamics (3.1) is passive.

3.1.4 Port-Hamiltonian for switching circuits

In [18] the port-Hamiltonian representation is applied to generalized switching circuits, such as buck and boost converters.

In [11] the formalism is applied to a VSC. The port-Hamiltonian form of general power electronic converter from the article is given as

$$\dot{x} = (\mathcal{J}_0 + \sum_{i=1}^{m} \mathcal{J}_i u_i - \mathcal{R}) \nabla \mathcal{H}(x) + (G_o + \sum_{i=1}^{m} G_i u_i) E, \tag{3.5}$$

with $x = \in \mathbb{R}^n$ the converter state. The interconnection matrix has been separated in two parts. One part consisting the terms directly affected by the control parameters, $u \in \mathbb{R}^m$ and conversely, one part not dependent by the control. $E \in \mathbb{R}^o$ is a vector representing the external sources that are included for describing the system. The input matrix $G \in \mathbb{R}^{n \times o}$ is divided into one a part unaffected by the control input and one which is affected.

3.2 The design of the PLLs

In order to avoid repetition, a general methodology concerning the design procedure is presented in this section. The methodology is applicable on all the case models represented in Chapter 2. The passive outputs–instrumental for the control design– are presented in Chapter 3.2.3.

The port-Hamiltonian representation and the calculation of the passive outputs consist of a high number of matrices. For the sake of compactness and readability, the least important matrices have been moved to the Appendix B, where, each PLL has its own section. Color codes have been used as an attempt to help separating the different PLLs. The original model has no color, while red is used for alternative 0, green for alternative 1 and finally blue for the alternative 2 model.

Briefly, the design of the PLLs is divided into four steps:

1. Represent the system under the Port-Hamiltonian formalism
2. Express the system using incremental variables [11]
3. Calculate $\tilde{y} = G_N^{\mathsf{T}}(x)Q\tilde{x}$, with $G_N(x) = [\mathcal{J}_i Qx, \ldots, \mathcal{J}_m Qx]$ and simplify
4. Apply a PI to the passive output

Step two and three are merged into one step, by help of [11]. In order to better understand the effects of the theory, it is decided to apply the methodology on the equations derived from the traditional modeling (ch. 2.3.1) as well, even if the synchronization dynamics are not considered, as it assumes that ω_{pll} and ω_{g} are equal.

In Chapter 2, the different systems are expressed in SRF.

- Traditional $\rightarrow$ Eq. (2.10) - Eq. (2.12)
- Alternative 0 $\rightarrow$ Eq. (2.14) - Eq. (2.17)
- Alternative 1 $\rightarrow$ Eq. (2.18) - Eq. (2.21)
- Alternative 2 $\rightarrow$ Eq. (2.22) - Eq. (2.25)

These equations are the base for the port-Hamiltonian representation of each of the models of interest.

3.2.1 Port-Hamiltonian

Unfortunately, the synchronization model of the 2L-VSC of interest cannot be directly described by means of the port-Hamiltonian form (3.5) introduced in [11], in its shape. This is due to the following two facts:

1. The *trigonometric nonlinearity* Eq. (2.8) introduces a state-dependent additional partition of the interconnection matrix; i.e., $\mathcal{J}(\delta)$. As seen in Eq. (3.5), the interconnection matrices $\mathcal{J}_0$, and $\mathcal{J}_i$ are not state-dependent. Thus, the PI stabilization result from [11] cannot be directly applied. It is therefore decided to approximate Eq. (2.8) to the identity matrix such that $\mathcal{J}(\delta)$ has no terms including δ. The same

implies for the G_0 matrix for the alternative 2 model, because the *trionometric nonlinearity* occurs describing the grid.

2. Treating ω_{pll} as a control parameter instead of an input also results in a 7$^{\text{th}}$ differential equation that is related to the difference between ω_{pll} and ω_{g}—see for example (2.25). More importantly, in this equation the control variable ω_{pll} enters linearly, unlike u in (3.5).

Hence, the port-Hamiltonian form presented and validated in [11] needs to be extended and validated to include the second point before any PLL alternatives can be designed. The port-Hamiltonian model needed to represent the system of this work is now

$$\dot{x} = (\mathcal{J}_0 + \sum_{i=1}^{m} \mathcal{J}_i u_i - \mathcal{R})\nabla\mathcal{H}(x) + (G_o + \sum_{i=1}^{m} G_i u_i)E + G_\omega u, \tag{3.6}$$

where the product between $G_\omega \in \mathbb{R}^{n\times m}$ and u is indeed the linear entry of the control variable ω_{pll} in the 7$^{\text{th}}$ differential equation. The validation of stability proof concerning this extension is given in Appendix A.

In order to represent the system with the port-Hamiltonian formalism, the first step is to locate the states of the system in addition to the (open-loop) control variables. For the traditional system, 6 differential equations are used to describe the system, while 7 differential equations are used for the alternative systems capturing the synchronization dynamics. Equation (3.7) represents all the states for the alternative models, whereas δ is the additional state distinguishing the traditional case from the alternatives.

$$x = \begin{bmatrix} i_{v,d} & i_{v,q} & v_{f,d} & v_{f,q} & i_{g,d} & i_{g,q} & \delta \end{bmatrix}^\top \tag{3.7}$$

Furthermore, the control variables are identified. For the traditional model, e_d and e_q are the only control variables. For the alternative models, ω_{pll} is additionally treated as a control parameter. Eq. (3.8) describes the different control parameters for the alternative models.

$$u = \begin{bmatrix} \omega_{\text{pll}} & m_d & m_q \end{bmatrix}^\top \tag{3.8}$$

The control variables e_d and e_q are the output voltages of the VSC in the SRF. In this work e_d and e_q are controlled indirectly by the modulation indices m_d and m_q, respectively, through the linear relationship

$$e_d = V_{DC} \cdot m_d,$$

$$e_q = V_{DC} \cdot m_q,$$

with V_{DC} the constant dc voltage source of the VSC.

Moreover, the external source vector E affecting the system is identified. For all the cases, the external sources remain the same. The external sources are considered as constant disturbances, and therefore not possible to influence. The external source vector affecting the models is given in Eq. (3.9), with V_{DC} the constant DC-voltage source, $V_{g,d}$

and $V_{g,q}$ are the grid voltage in SRF and ω_g is the (a priori unknown) angular frequency of the grid.

$$E = \begin{bmatrix} V_{DC} & V_{g,d} & V_{g,q} & \omega_g \end{bmatrix}^\top \tag{3.9}$$

The remaining part is to identify the different matrices. The different port-Hamiltonian matrices are shown in:

- Traditional → Appendix B.1.1
- Alternative 0 → Appendix B.2.1
- Alternative 1 → Appendix B.3.1
- Alternative 2 → Appendix B.4.1

3.2.2 Passivity on Incremental Model

Following the result in [11], the passive output of the system is defined as:

$$\tilde{y} = G_N^\top(x) Q \tilde{x}$$

Were Q$\tilde{x}$ is the multiplication of the Q-matrix, which is a $n \times n$ matrix that in the diagonal includes 1 divided by the storage units of each differential equation. In addition, $\tilde{x}$ is a vector including the incremental state variables and G_N equals:

$$G_N(x) := [J_1 Q x + G_1 E | ... | J_m Q x + G_m E]$$

The required matrices for calculating the passive output are given in:

- Traditional → Appendix B.1.2
- Alternative 0 → Appendix B.2.2
- Alternative 1 → Appendix B.3.2
- Alternative 2 → Appendix B.4.2

3.2.3 Passive output for the different models

Traditional

An interesting result of the passive output of the traditional model is the fact that one recovers the standard current controller error, where $i_{v,d}^*$ and $i_{v,q}^*$ are the current references. It is worth mentioning however that the current controller in the specialization project [1] includes a feed-forward term and decoupling terms. In order to make the equations as similar to the simulations possible, the cross-coupling and feed-forward terms have been removed. The passive output of the traditional model is described by Eq. (3.10).

$$\tilde{y} = \begin{bmatrix} V_{DC}(i_{v,d} - i_{v,d}^*) \\ V_{DC}(i_{v,q} - i_{v,q}^*) \end{bmatrix} \tag{3.10}$$

Alternative 0

For this model, the passive output is of the form (3.11). It can be seen that an additional row is included in the passive output vector,which is related to the output of the control variable ω_{pll}. Moreover, the red term is a result *bilinear product nonlinearity*, while the other term is related to the fact that ω_{pll} and ω_{g} are treated as unequal values.

The currents $i_{v,d}$ and $i_{v,q}$ are the only states related to ω_{pll} in this model.

$$\tilde{y} = \begin{bmatrix} L_f(i_{v,d}i^*_{v,q} - i_{v,q}i^*_{v,d}) + \tau(\delta - \delta^*) \\ V_{DC}(i_{v,d} - i^*_{v,d}) \\ V_{DC}(i_{v,q} - i^*_{v,q}) \end{bmatrix} \tag{3.11}$$

Alternative 1

The passive output related to the alternative 1 model is illustrated in Eq. (3.12). Compared to the alternative 0 passive output, the alternative 1 model has one additional term in the first row of the vector. This is because in addition to $i_{v,d}$ and $i_{v,q}$ being multiplied by ω_{pll} in the state-space model, the two states $v_{f,d}$ and $v_{f,q}$ are also being multiplied by ω_{pll}.

$$\tilde{y} = \begin{bmatrix} L_f(i_{v,d}i^*_{v,q} - i_{v,q}i^*_{v,d}) + C_f(v_{f,d}v^*_{f,q} - v_{f,q}v^*_{f,d}) + \tau(\delta - \delta^*) \\ V_{DC}(i_{v,d} - i^*_{v,d}) \\ V_{DC}(i_{v,q} - i^*_{v,q}) \end{bmatrix} \tag{3.12}$$

Alternative 2

The passive output related to the alternative 2 model is shown in Eq. (3.13). Finally, in the alternative 2 model, all the states are related to the output of ω_{pll}. Thus, $i_{g,d}$ and $i_{g,q}$ additionally are related to ω_{pll} compared to the alternative 1 model.

$$\tilde{y} = \begin{bmatrix} L_f(i_{v,d}i^*_{v,q} - i_{v,q}i^*_{v,d}) + C_f(v_{f,d}v^*_{f,q} - v_{f,q}v^*_{f,d}) + L_g(i_{g,d}i^*_{g,q} - i_{g,q}i^*_{g,d}) + \tau(\delta - \delta^*) \\ V_{DC}(i_{v,d} - i^*_{v,d}) \\ V_{DC}(i_{v,q} - i^*_{v,q}) \end{bmatrix} \tag{3.13}$$

3.2.4 PI stabilization

As prooved in [17], the passive outputs can be used to stabilize the power electronics-based system by means of simple PI controllers. This yields three additional states, related to the integral part of the controller, where two of the states are related to the PI controller of the current control, while the third state is related to the PI controller of the PLL. The PI controllers in the current controller stay the same for all the cases, while the input to the PI controller defining the output of ω_{pll} changes for each case, as each case has a different first row of the passive output vector. In this work, the three different states are called A,B and C. Whereas A is the state related to the d- component in the current controller, B is related to the PLL and C is related to the q-component in the current controller. The new states can be described by the PI Eq. (3.14).

$$\begin{aligned} \dot{z} &= -\tilde{y} \\ u &= -K_p\tilde{y} + K_i z \end{aligned} \tag{3.14}$$

Where $\tilde{y}$ is the passivity vector, u is the control vector and K_p and K_i are the PI parameters depending on the controller. The values of K_p and K_i are provided in Table 2.1. Ideally, the different PLLs should have different PI parameters due to properly take into account their differences. However, this has not been prioritized in this work.

3.3 Discussion

One challenge related to the new terms is the dependency on the calculated steady state values. The more terms related to ω_{PLL}, the more steady state values have to be calculated and fed into the PLL. The alternative PLLs also input the measured values of the different states in the SRF. The amount of state values needed is also depending on how much of the system is referred to the SRF rotating at ω_{pll}. One weakness of the steady state values used in the control is that their precise calculation requires knowledge of all the system parameters, such as the external source vector. This includes the grid voltage and grid frequency as well as the DC-voltage. In reality, these values are not known at each instant. How much knowing these values affects the steady state calculations has not been quantified in this work.
Additionally, the calculation of the steady state values as well as the measurement of the grid current have to be done without invalidating the Lyapunov stability proof. Tools such as a micro PMU can be used to measure the grid current, but challenges related to the sampling time and the resolution might occur [19] [20].

The total stored energy of the system analysed in this work can be described by Eq. (3.15.

$$\mathcal{V}(x) = \frac{1}{2}\tilde{x}^\top Q\tilde{x} \tag{3.15}$$

where $\tilde{x} = x - x^*$ and the Q-matrix is an $n \times n$ matrix that in the diagonal includes 1 divided by the storage units of each differential equation. The storage units in this system is the inductors and capacitors. The stored energy of the system will decrease over time due to the energy storage characteristics of the components. Hence, the derivative of the system is expressed by

$$\dot{\mathcal{V}} \leq \tilde{y}^\top \tilde{u} \tag{3.16}$$

where $\tilde{y}^\top$ is the passivity output and $\tilde{u}$ is the control input. Chapter 3.1.1 and 3.1.2 presents the definition of a Lyapunov function and an asymptotic stable system. Eq. (3.15) and Eq. (3.16) satisfies the restriction for a Lyapunov function and an asymptotic stable system. Hence, the passive outputs designed in this work come with a stability certificate I.e the Lyapunov function. Therefore, can the PLLs be categorised as large signal stable.

Chapter 4

Performance Analysis

In this chapter, a standard PLL–referred to in this document as the traditional PLL– illustrated in Figure 2.4 is compared to the alternative PLLs with respect to the overall performance and stability. The parameter values are given in Table 2.1. Despite of not being optimally tuned, the performance and the stability characteristics of the different PLLs are compared nonetheless. All the simulations have been conducted by help of MATLAB. Except the model referred to as alternative 1, the mathematical equations used for the control design are validated by means of a MATLAB function in MATLAB Simulink.

4.1 Continuous- Validation

For simplicity, most of the simulations have been conducted with a continuous voltage source, instead of the generated voltage source from the PWM. This reduces the computational cost of the simulations in addition to remove any uncertainties regarding the PWM signals. An advantage with this is the possibility to conduct continuous simulations rather than discrete.
The validation of the continuous model and the model, including PWM signals, are exclusively done for the original model. Because such validation has already been made in [21] [22]. The continuous model is sufficient if the transient response of the two models equal. The simulation event consist on a step change of $i_{v,d}$ from 10 A to 5 A, and all the six states are compared. This includes the converter current, $i_{v,d}$ and $i_{v,q}$, together with the voltage across the capacitors, $v_{f,d}$ and $v_{f,q}$, as well as the grid current, $i_{g,d}$ and $i_{g,q}$ all in the synchronous reference frame.

4.1.1 Validation Results

Figure 4.1 illustrates the different states throughout the simulation. In order to distinguish between the transient response of the simulations, a small transient window is included in the subfigures.

Figure 4.1a shows the converter current in the synchronous reference frame. Due to the high ripple in the current, it is hard to distinguish if the transient responses match. Nevertheless, both the continuous and the discontinuous d-component of the current follow the reference. The q-component of the current is equal to zero for both cases.

As well as the converter current, the grid current by use of PWM oscillates more. Despite this, the transient responses of the continuous and discontinuous models match. This can be seen in Figure 4.1b.

Figure 4.1c illustrates the voltage across the capacitor in the synchronous reference frame. From the figure, it can be seen that transient response correlates for both the cases.

The match between the simulations is considered as sufficient, hence the continuous model is used whenever possible.

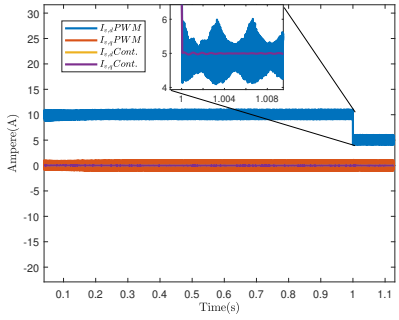

(a) i_v

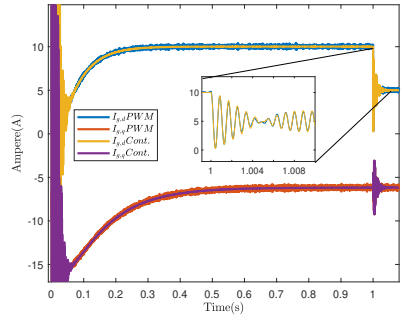

(b) i_g

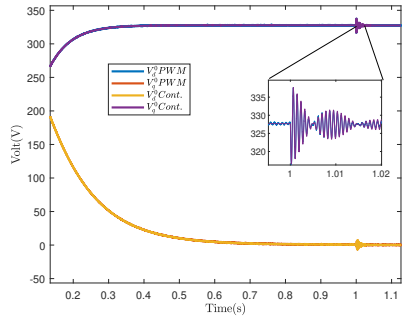

(c) v_f

Figure 4.1: Continuous and discrete comparison of the different states.

4.2 Performance

This section represents and compares the different PLLs, with respect to the performance. Mainly, the responses of the states are illustrated and commented when the reference cur-

rent in the current controller is changed from 10 A to 5 A.
For each of the different cases, the steady state values are calculated in MATLAB scripts. The script used for the alternative 1 model is illustrated in Appendix G. A total of seven differential equations are describing the system, and the total of unknowns in the system is ten, implying that three parameters can be set as desired references in order to calculate a steady state condition. In this work the values $i_{v,d}^{\text{ref}} = 10A$, $i_{v,q}^{\text{ref}} = 0A$ and $\delta^{\text{ref}} = 0$ are chosen. As presented in Chapter 3, the alternative PLLs are using the steady state values as part of their control. Hence, the calculation of the parameters has to be sufficiently accurate in order to fulfill the Lyapunov stability criteria.

As introduced in Chapter 1, $v_{f,q}$ cannot be estimated to 0 at each instant in a weak grid.
As a first approach, all the PLLs of this work included the estimation that

$$\delta = \arctan\left(\frac{V_{f,q}^m}{V_{f,d}^m}\right),$$

resulting in some challenges related to the validation of the models, and therefore the estimation is not sufficient for the scope of the work. Due to lack of time, the real δ is used instead, even if this measurement, in reality, is not available. The method of providing the real δ is explained in Chapter 2.3.6.

Having the real value of δ establishes the possibility to focus on the contribution from the non-linear terms. Nevertheless, simulations with the estimation of δ are conducted, even though the models could not be validated. These simulation results are included in Appendix C for being able to compare the results. All the simulation results, except the alternative 1 case, includes the simulation results from the build in MATLAB function.

4.2.1 Built in MATLAB function

The MATLAB function was also used in the specialization project [1]. The advantage with the MATLAB function is to simulate the equations with respect to time. Implying that the systems under investigation can be simulated based soly on their mathematical description. If the response of the mathematical simulation and the MATLAB Simulink simulation matches, the equations are validated. If the equations are validated, the same validation applies for the stability analysis. Due to the fact that the MATLAB function excludes the switching of the VSC, the function shows the desired response of the system without any switching dynamics.

4.2.2 Performance Results

Table 4.1 illustrated the steady state values calculated in different MATLAB scripts. From the table, it can be seen that the steady state values for the original-, alternative 0- and alternative 1- model equals. For some reason, the steady state for the alternative 2 model are slightly different from the other models. It can also be seen that for the alternative 2 model, δ does not equal zero.

The different states are compared in order to compare the different PLLs. Figure 4.2 illustrates the converter current for the four different cases. Except the alternative 1 model,

Table 4.1: Comparison of the calculated steady state values.

State	**Original**	**Alt 0**	**Alt 1**	**Alt 2**	**Unit**
$i_{v,d}$	10	10	10	10	[A]
$i_{v,q}$	0	0	0	0	[A]
$v_{f,d}$	327.6814	327.6814	327.6814	327.0977	[V]
$v_{f,q}$	0.6348	0.6348	0.6348	-1.9286	[V]
$i_{g,d}$	10.012	10.012	10.012	10	[A]
$i_{g,q}$	-6.1766	-6.1766	-6.1766	-0.0062	[A]
δ	0	0	0	-0.003	[-]
A	0.0072	0.0072	0.0072	0.0072	[-]
B	0.2186	0.2186	0.2186	0.2186	[-]
C	0.0003	0.0003	0.0003	0.0002	[-]

the simulations include the comparison with the MATLAB function simulation. The MATLAB function simulation and the system simulation correlates for all the different cases. In the transient response, the small differences between the function and the system can be seen. The transient response for the different PLL seems to be somewhat the same. Because of the alternative 2 model are simulated including the PWM, the simulations include more ripple.
Further, the third and fourth state in the system are compared with respect to performance. $v_{f,d}$ and $v_{f,q}$ differs more compared to the converter current. The alternative 1 and alternative 2 models tend to be closer to the steady state values at each instant in the early stage of the synchronization. This can, however, be related to the lack of optimal tuning for the PI parameters. The transient response for the different PLLs are somewhat the same.
Figure 4.4 illustrates the grid current in SRF during the simulation. It can be seen that the alternative 0 and alternative 2 correlates more to the function compared to the original model. The figure also illustrates how the alternative 1 model almost equal the step response, while the other models have a small transient response.

With respect to the performance, the alternative PLLs do not show significant improvement with these simulations. Due to lack of time, simulations including an increasing grid inductance were not conducted. An increasing grid inductance would perhaps reveal some possible differences.

Challenges faced

Due to an algebraic loop, some of the simulations are conducted with the discontinuous model including the PWM. The error message mainly occurred related to the park transformations in the simulations. Nevertheless, the continuous model is used if possible.
Unfortunately, the MATLAB function and the alternative 1 model are not matching. Consequently, this yields a certain uncertainly regarding all the results related to the alternative 1 model.
A third challenge faced is related to the simulations concerning the simulations with the estimated δ. These simulations are shown in the appendix, and will not be the main focus

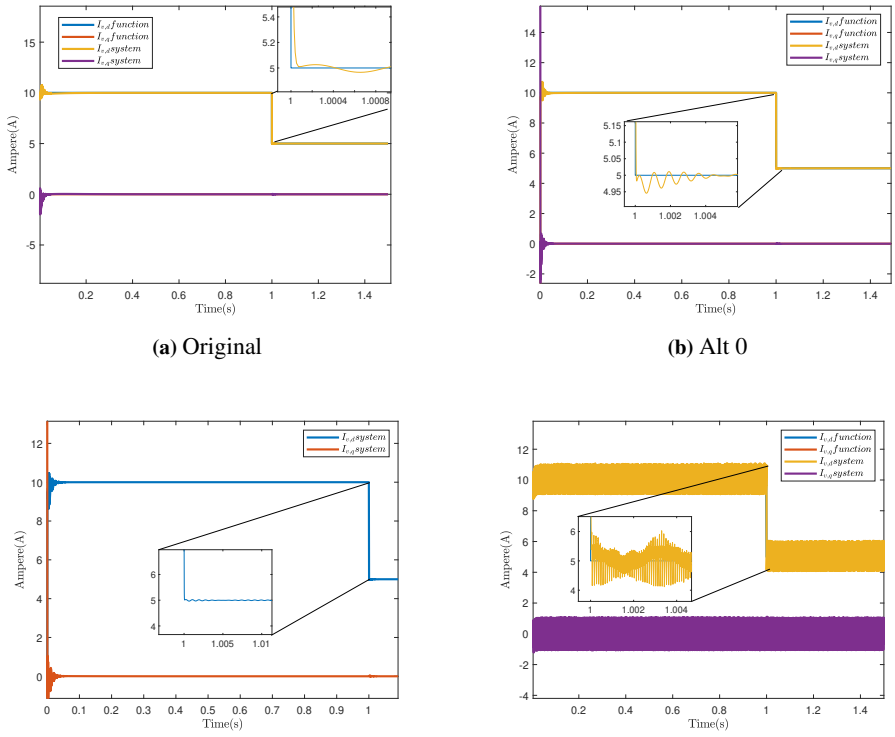

(a) Original

(b) Alt 0

(c) Alt 1

(d) Alt 2

Figure 4.2: $i_{v,d}$ and $I_{v,q}$ comparison of the different models. δ known.

in this work. Nevertheless, these challenges are present as long as the PLLs designed in this work are used.

The alternative 1 and alternative 2 PLLs manage to locate different steady state values for $v_{f,d}$ and $v_{f,q}$, hence also $i_{g,d}$ and $i_{g,q}$ in order to maintain the power flow. From an operating point of view, the systems seem stable. However, if a gain of -1 is added in front of the PI controller, the steady state values correlates with the calculated values. Adding a gain of -1 on the alternative 1 PLL yields an improved result, while the alternative 2 model faces some problems. The alternative model 2 system is now unstable at 10A, but when the reference value of $i_{v,d}$ is changed to 5 A the system stabilizes.

4.3 Small Signal Stability

One way of comparing the different PLLs is by the use of small signal stability. In small signal stability, the power system is analysed after a small disturbance is subjected to the system. If the oscillations caused by the disturbance is suppressed such that the deviations of the system state variables remain small for a long time, the system is stable. Hence, if

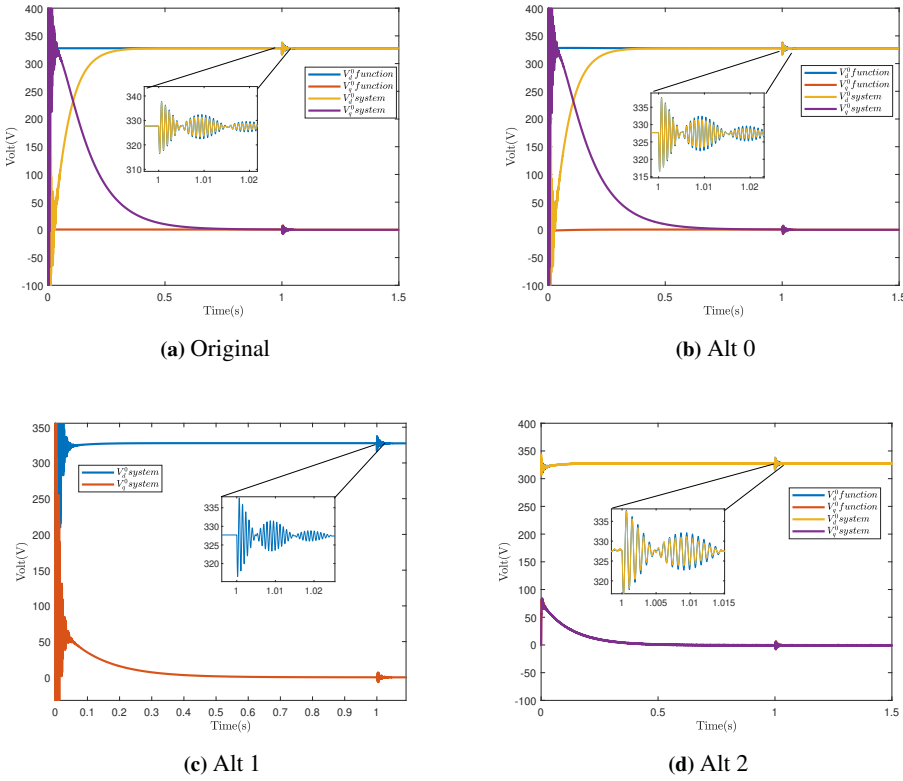

(a) Original

(b) Alt 0

(c) Alt 1

(d) Alt 2

Figure 4.3: $v_{f,d}$ and $v_{f,q}$ comparison of the different models. δ known.

the magnitude of the oscillations continues to increase or sustain indefinitely, the system is unstable [23].
In order to conduct small signal stability, it is convenient to represent the system on state space representation. For a linear system, the state space representation is:

$$\begin{aligned} \dot{x} &= Ax + Bu \\ y &= Cx + Du \end{aligned} \tag{4.1}$$

where A, B, C and D are matrices, $\dot{x}$ are the states, and u represents the inputs. For a nonlinear system, however, the system state space representation is illustrated in Eq. (4.2). The system simulated in this work is a nonlinear system, but for the small signal analysis the system is linearized. When small changes are applied to the systems, the linearization is a sufficient representation. A representation of a nonlinear system is more complex compared to a linear. Generally, a nonlinear system can be described by Eq.(4.2).

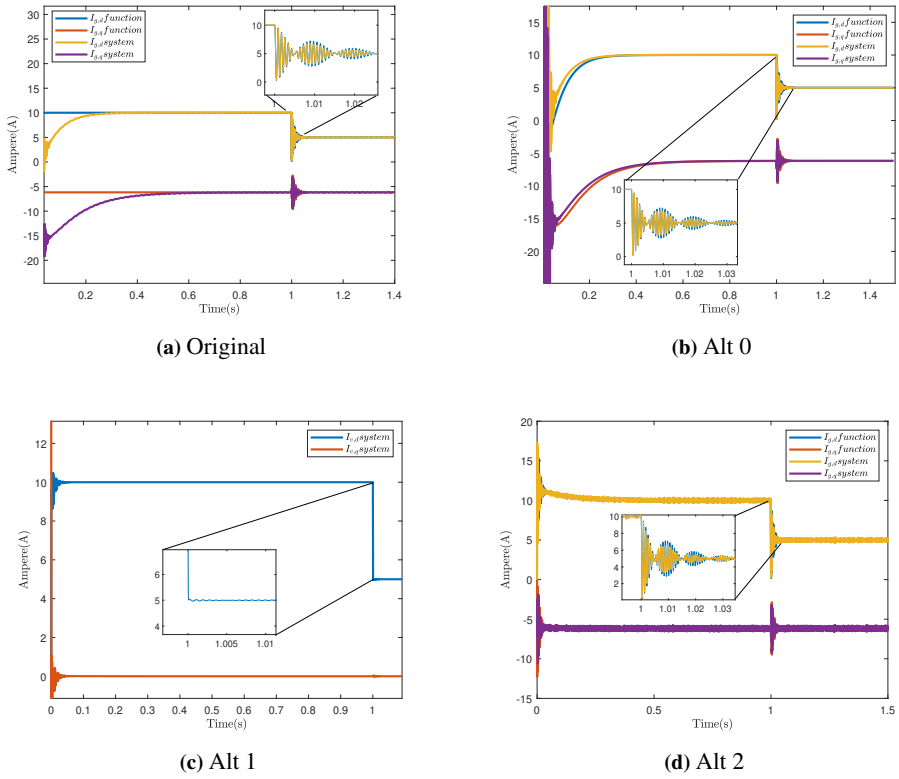

(a) Original

(b) Alt 0

(c) Alt 1

(d) Alt 2

Figure 4.4: $i_{g,d}$ and $i_{g,q}$ comparison of the different models. δ known.

$$
\begin{aligned}
\dot{x_1} &= f_1(x_1, ..., x_n) + g_1(x_1, ..., x_n)u \\
&\vdots \\
\dot{x_n} &= f_n(x_1, ..., x_n) + g_n(x_1, ..., x_n)u \\
y &= h(x)
\end{aligned}
\tag{4.2}
$$

Where $\dot{x_1}, ..., \dot{x_n}$ are the state variables, u represents the input and y is the output.

For the state space model deducted in this work, [24] are used as an inspirational source. Unlike [24], this work does not include a power-controller, but despite this the model in article correlates to the model in this work.

4.3.1 Method

In order to conduct a small signal stability analysis for all the models, a script for each of the different systems is made. This yields in total four different MATLAB scripts. One for the original PLL, and one for each of the alternative PLLs. The first step of the stability

analysis is to calculate the steady state values including the references.
A script is made in order to determine the steady state values of the different systems. The scripts include a function with the ten differential equations describing the respectively systems in closed loop. Thus, the difference between the different scripts is the contribution from the PLL and the results of applying different park-transformations. The script related to the alternative 1 model is illustrated in Appendix G. As a result of the passivity-based controller, the control parameters, e_d, e_q and ω_{pll}, are substituted with the passivity-based controller designed for each case. This means that PI stabilization is applied on the different terms as discussed in Chapter 3.2.3.

In order to get the steady state values, all the different equation describing the closed loop system are included in a script. The steady state values calculated from this MATLAB script have different attributes depending on the complexity of the PLLs. The basic PLL does not include the steady state values in its control, while the passivity-based controllers do. The dependency of the steady state values is increasing the more of the states that are related to ω_{pll}. Hence, the alternative 2 PLL is dependent on the steady state values for the converter current, the voltage across the capacitor in addition to the grid current. By contrast, the converter side currents in steady state are the only states alternative 0 is depending on.
After the steady state values are calculated, the linear state space representation of the model can be made. In order to linearize the system, the A, B, C and D matrices have to be determined. The A and B matrix are calculated by help of a MATLAB code. The equations for the A and B matrices are illustrated in Eq. (4.3) and Eq. (4.4). The C matrix for this system is the identity matrix, while the D-matrix is not excising in this system [25].

$$A = \begin{bmatrix} \frac{\partial f_1}{\partial x_1} & \cdots & \frac{\partial f_1}{\partial x_n} \\ \vdots & & \vdots \\ \frac{\partial f_n}{\partial x_1} & \cdots & \frac{\partial f_n}{\partial x_n} \end{bmatrix}_{x=x^*} \tag{4.3}$$

$$B = \begin{bmatrix} \frac{\partial f_1}{\partial y_1} & \cdots & \frac{\partial f_1}{\partial y_n} \\ \vdots & & \vdots \\ \frac{\partial f_n}{\partial y_1} & \cdots & \frac{\partial f_n}{\partial y_n} \end{bmatrix}_{x=x^*} \tag{4.4}$$

The A matrix is the partial derivative of the function with respect on the states, while the B matrix is the partial derivative of the function with respect on the input parameters. Both the matrices are evaluated at the equilibrium points.

By knowledge of the A matrix, the eigenvalues of the different systems can be calculated. In this work, the eigenvalues were calculated by help of a build in MATLAB code.

4.3.2 Eigenvalues

The dynamic behavior of a system is dependent on the system's eigenvalues. A large class of nonlinear systems can be described on the form illustrated in Eq. 4.2, and hence by a linearization of the system described in Eq. (4.1). A linearization is sufficient for small variable changes. If A is an n-by-n matrix, the n numbers λ that satisfy Eq. (4.5) are the eigenvalues of A [26].

$$Ax = \lambda x \tag{4.5}$$

The eigenvalues can be computed by calculating the roots of Eq. (4.6).

$$det(s\mathbf{I} - \mathbf{A}) = 0 \tag{4.6}$$

The numbers of eigenvalues are always the same as the dimensions of the A matrix. The eigenvalues can also be complex, and therefore it is usefully to depict them into the complex plane. The real part of the eigenvalue relates to the damping of the system, and in addition, the signs can tell if the system is stable or unstable. An eigenvalue can be defined as,

$$\lambda = \sigma + j\omega$$

where ω is the angle speed, and σ is the damping constant. In order for the system to be stable, the damping constant, σ, have to be less than zero [27].
In this work a MATLAB code has been used to calculate the eigenvalues based on the knowledge of the A-matrix. Each of the different models have their own script calculating the eigenvalues and participation factors. The alternative 1 script is illustrated in Appendix H.

4.3.3 Participation Factor

For each eigenvalue there exists a left and a right eigenvector. The right eigenvalue measures the activity of the state in the eigenvalue, while the left indicates how able the state is to influence the eigenvalue [27].

By combining the right and left eigenvector, it is possible to measure the association between the state variable and the modes. This combination is called the participation factor. Hence, knowing the participation factor, and therefore, knowing the states associated with the critical eigenvalues, simplifies the tuning process.
In order to conduct simulations and get valid comparison results, the systems have to be stable. Due to the different PLLs, individual analyses were made for each system.
The equations used for calculation of the participation are Eq.(4.7) and Eq.(4.8), respectively. The methodology for the participation factor analysis is heavily based on [27] and [28].

$$P = \begin{bmatrix} P_1 & P_2 & \cdots & P_n \end{bmatrix} \tag{4.7}$$

$$P_i = \begin{bmatrix} P_{1i} \\ P_{2i} \\ \vdots \\ P_{ni} \end{bmatrix} = \begin{bmatrix} \phi_{1i}\Psi_{i1} \\ \phi_{2i}\Psi_{i2} \\ \vdots \\ \phi_{ni}\Psi_{in} \end{bmatrix} \tag{4.8}$$

P is a nxn matrix, describing the participation factor of each state for all the different eigenvalues. P1, for example, is a nx1 vector, were the sum equals 1, and the different rows in the vector describes the participation of each state. ϕ is the right eigenvector, while Ψ is the left.

4.4 On the small-signal stability results

Throughout the work the simulations conducted in MATLAB Simulink and the calculations have had small mismatches. Due to lack of time, the trouble causing the mismatch has not been identified, which yields uncertainties with the work. Due to the fact that the PLLs are working in the Simulink environment while the equations indicate that the systems are unstable. It is decided to trust the Simulink simulations. Because this work balancing between theory and practice, it is chosen to have a more practical approach on the discussion of the results. Leaving the eigenvalue analysis and the participation factors only as indicative results. The stability results where δ is known, are shown in Appendix D. Additionally, the stability results where δ is estimated are shown in Appendix E

Chapter 5

δ-independent synchronization

Throughout the work the challenges related to the *angle difference state δ unavailability* have been present. A solution to the challenge might have been discovered in the late work of the thesis. This chapter focuses on this solution and also function as a discussion chapter.

5.1 Design

Due to the challenge regarding the δ term, the tuning parameter τ is increased and decreased in order to locate the effect of the term related to δ. During this analysis, it was found that the term τ can be chosen arbitrarily small such that it still appears in the Lyapunov function presented in chapter 3.3 is still valid. However, from a practical perspective, arbitrarily small τ removes the contribution of the term associated to the unavailable angle δ. Recall that, as discussed in Chapter 2.2, τ decides the contribution of δ in the input of the PI controller in the PLL.

First consider the traditional PLL shown in Figure 2.3. Indeed, removing the term related to δ in the PLL results in a PLL excluding internal feedback.

By contrast, both the systems including the alternative 1 and alternative 2 PLL operates well without the δ term included; i.e., with an arbitrarily small τ. The alternative 1 PLL does not include the measurement and the steady state calculation of the grid current, which is the argument that favors the alternative 1 PLL over the alternative 2 PLL. The cost of the alternative 1 might be lower due to the fact that the PLL does not need information about the grid current. The grid current can be measured by use of for example a micro PMU, whereas challenges related to the sampling time and resolution might occur [19] [20].

However, both the alternative 1 and alternative 2 PLL still require a somewhat correct estimation of the steady state values, and therefore have some robustness issues.
On the other hand, the performance of the alternative 1 and alternative 2 model seem to work with poorly estimation of the steady state currents. The alternative 2 model requires the steady state values of $i_{g,d}$ and $i_{g,q}$, but throughout the work it is discovered that the

performance are almost unaffected by poorly calculated steady state values for the currents.

Both the systems operate poorly when $v^*_{f,d}$ and $v^*_{f,q}$ are poorly estimated. An advantage by removing the term related to δ is that the control does no longer depend on δ^*, resulting in $v^*_{f,q}$ can be chosen to zero instead, and the two steady state voltages are therefore known. Another advantage of having $v_{f,q}$ forced to zero is the easy power flow control with the direct relationship of $i_{v,d}$ and active power, and $i_{v,q}$ and reactive power described in Chapter 2.2.

5.2 Results

In order to best compare the new PLL to the previous PLLs, the same procedure regarding the tests is done. This includes steady state calculations, performance simulations and stability analysis.
A result of excluding the term related to δ, $v^*_{f,q}$ can be directly established to any desired reference. The three control references of this new PLL are then $i^*_{v,d}$, $i^*_{v,q}$ and $v^*_{f,q}$. In Table 5.1 the steady state values are illustrated. The table shows that all the control parameters equal the reference values. Unlike the steady state calculations in the previous chapter (except alternative 2), δ does not equal 0 in steady state.

Table 5.1: Steady state calculations when δ is removed

State	Value	Unit
$i_{v,d}$	10	[A]
$i_{v,q}$	0	[A]
$v_{f,d}$	327.6802	[V]
$v_{f,q}$	0	[V]
$i_{g,d}$	10.012	[A]
$i_{g,q}$	-6.1572	[A]
δ	-0.0019	[-]
A	0.0072	[-]
B	0.2186	[-]
C	0.0003	[-]

In order to compare the result with the performance results from Chapter 4, the same step has been made. After 1 second, $i^{\text{ref}}_{v,d}$ is changed from 10A to 5A. A zoomed window of the transient response is included in each of the sub-figures.

Figure 5.1 illustrates the different states throughout the simulation. It can be seen that the states are unaffected by removing the term related to δ. The system shows a sufficient transient response when the change occurs. The PLL uses around 0.5 second to get $v_{f,q}$ equal zero, which by improved tuning will most likely be lower. Nevertheless, due to lack of time these simulations were not validated by neither equations nor the build in MATLAB function.

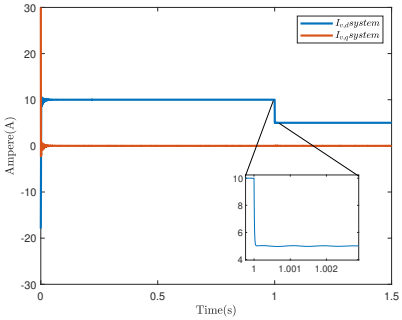

(a) i_v

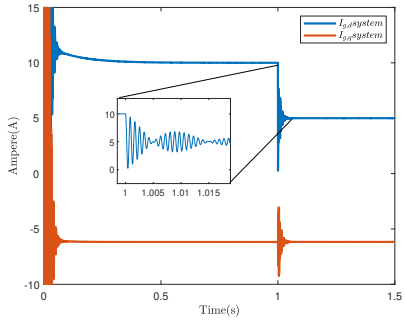

(b) i_g

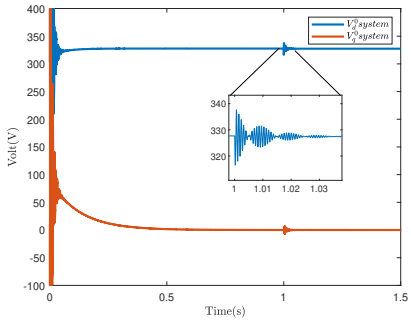

(c) v_f

Figure 5.1: States in alt.1 model when δ is removed.

Even though the simulation results excluding the term related to δ nor the small signal stability analysis could be validated, all the alternative models are mathematically validated. Which in theory ensures large signal stability because of the Lyapunov function. This property is highly valuable, and also very attractive in the future energy systems. By conducting more simulations, in addition to test the PLLs in the National Smart Grid Laboratory, the PLLs can within a short period of time be applied in the industry.

Throughout this work the challenges related to the *bilinear products nonlinearity* and *angle difference state unavailability* have been solved. The remaining challenge is related to the *trigonometric nonlinearity*, and in [29] this challenge is investigated. The article investigates the possibility to obtain a globally asymptotic stable system, with a restriction region of the tuning parameters in the PI controller. Hence, the PLL will have a region where all parameter values are stable. This naturally limit the PLL in some extent, but how much this limit the performance is unknown.

Chapter 6

Conclusion and Further Work

In the specialization project [1], three challenges related to the PLL were discovered, and are summarized below for convenience.

- *Trigonometric nonlinearity:* This nonlinearity appears since two different Park transformations at two different frequencies become necessary to describe the VSC synchronization dynamics; one associated with the frequency of the grid ω_{g}, while the other one associated with the frequency estimated by the PLL, ω_{PLL}.
- *Bilinear products nonlinearity:* This nonlinearity appears naturally when the estimated frequency ω_{PLL} is considered as a control variable instead of a constant. Thus, the cross-coupling terms in the VSC model will consist on a control variable multiplying a state variable.
- *Angle difference state unavailability:* A third problem related to the synchronization model of VSC is that the angle difference state variable $\delta \triangleq \theta_{\mathrm{PLL}} - \omega_{\mathrm{g}} t$ cannot be measured in the weak grid case, and therefore is unavailable for use in the control. This angle is indeed the difference between the two angles used in both Park transformations.

Both the *bilinear product nonlinearity* and the *angle difference state unavailability* are solved in this work. There are still restrictions related to these two problems. The only control parameters, for example, are at this point $i_{v,d}$, $i_{v,q}$ and δ. For the PLL presented in Chapter 5 the control of δ is substituted with $v_{f,q}$. Yielding some robustness issues.

6.1 Conclusion

In this master thesis the challenge related to the *bilinear product nonlinearity* in the synchronization model of the VSC is prioritized. This includes designing PLLs that are able to handle nonlinear systems, unlike the traditional PLLs currently in use today. The approach of solving the challenges related to the nonlinearities is based on Lyapunov theory

as well as passivity. In [11] the design of PI-Passivity-based control is applied to power electronics converter with *bilinear product nonlinearities*, although such a work did not consider any synchronization dynamics. In this master thesis however, the angular frequency provided by the PLL ω_{pll}, is treated as a control variable and hence unequal to the *a priori* unknown angular frequency of the grid ω_g. This more accurate interpretation creates an additional state describing the system. Hence, the equations used in [11] needed to be extended and slightly modified to fit the case of interest in order to apply the PI-PBC result and thus design the PLLs. Due to the fact that ω_{pll} is treated as a control variable, and different from ω_g, two park transformations have to be used in order to transform the system in two different synchronous reference frames. Three alternative PLLs have been designed, and what mainly distinguishes them is which SRF each states are related to.
The three different PLLs designed have been compared to a traditional PLL used in the industry today, with respect to performance and small-signal stability. Due to a mismatch between the small-signal stability analysis and the performance analysis, the results relating the performance have been emphasized in this work.
Finally, the third challenge regarding the PLL has been attempted to solve. This gave three different sets of results. One (unrealistic) result including simulations where δ is assumed known, one set of simulations where δ is estimated with the arctangent relationship between $v_{f,q}$ and $v_{f,d}$ and a third set of results where the term related to δ is chosen arbitrarily small such that the PLL can in principle be independent of δ without invalidating the stability proof.

Due to lack of time, neither the performance nor small-signal stability analysis were fully completed, hence it is too early to give a final recommendation regarding which of the PLL is favoured for industrial applications. That being said, the different PLLs and specially the PLL without the δ term shows promising results related to performance, as this last one seems to solve two of the three challenges listed throughout the thesis. The results show that despite of δ not being included in this last PLL, the system synchronizes rapidly. Furthermore, even though the small-signal stability results are treated as tentative, they indicate that the eigenvalues are neither significantly affected by the estimation of δ nor by removing the term. This might indicate that the instabilities might occur due to poorly tuned PI parameters related to the rest of the states.
Another interesting observation is regarding the operation with only the term related to $v_{f,q}$ and $v_{f,d}$ connected to the PLL. Meaning that both terms related to the grid current and the converter current can be poorly estimated, and the PLL will still synchronize.

The results from this master thesis indicate that an improved PLL can be designed to take into account the non-linear behaviour of the system. In order to determine if the PLLs designed in this work are indeed an improvement over traditional solutions, more simulations have to be conducted. Although, the work of the thesis might not directly result in an improved PLL, it paves the path to eventually be able to design them in the near future.

6.2 Further Work

Indeed, more simulations have to be conducted, including the more challenging case of a more complex system, rather than the isolated system used in this work. In addition, focus on weaker grids is recommended where the grid inductance is increased. Unfortunately, time constraints and the COVID19 situation put a stop on all hope of testing the most promising PLL in the National Smart Grid Laboratory. Albeit advantageous, the knowledge of the external sources (necessary for a precise estimation of the equilibrium point) should gradually decrease for realistic implementations. Hence, the effects of not having complete knowledge of the grid can be considered in future designs.

Changing the reference values for the converter current can also yield some interesting results. This is due to the fact that the same reference values have been used in this work, and therefore the simulations are narrow in the extent of the varieties in the grid. This can provide some interesting results regarding the performance contribution from the passivity terms appearing in the PLL. With a higher variety of reference values, the importance of the different passivity terms could be studied in more depth. Removing the term related to δ might have more influence than what has been observed in this work; hence it is convenient to conduct more simulations where the term is both included and excluded. The performance might also show significant improvement with the parameters of the PI controller being optimally tuned.

As already stated, the PLL has three challenges that should be solved. Hopefully, the path towards solving two of these challenges have been addressed in this thesis, while the last problem was not considered here due to the complexity of handling *trigonometric nonlinearities*.

That being said, [29] investigates the possibility to solve this remaining problem where conditions for obtaining global asymptotic stability are found and imposed in the tuning of the PI parameters.
In order to fully trust the nonlinear equations used in the control design, obtaining a time-domain match between them and the simulations is of paramount importance.

Despite of the alternative 1 PLL being favored in this work, both the alternative 0 and alternative 2 PLL should be included in the procedure of designing an improved PLL. Because they may inherent characteristics that is favorable.

Bibliography

[1] Rune Steig. Model-based control of plug-and-play grid-connected inverters. Project report in TTM4502, Department of Information Security and Communication Technology, NTNU – Norwegian University of Science and Technology, Dec. 2019.

[2] Hannah Ritchie and Max Roser. Access to energy. *Our World in Data*, 2020. https://ourworldindata.org/energy-access.

[3] United Nations Climate Change. The paris agreement. [Accessed: 03- Mar- 2020].

[4] Dolf Gielen, Francisco Boshell, Deger Saygin, Morgan D. Bazilian, Nicholas Wagner, and Ricardo Gorini. The role of renewable energy in the global energy transformation. *Energy Strategy Reviews*, 24:38 – 50, 2019.

[5] T. Ericsen, N. Hingorani, and Y. Khersonsky. Power electronics and future marine electrical systems. *IEEE Transactions on Industry Applications*, 42(1):155–163, 2006.

[6] Jie Wu, Zhi-Xin Wang, Lie Xu, and Guo-Qiang Wang. Key technologies of vsc-hvdc and its application on offshore wind farm in china. *Renewable and Sustainable Energy Reviews*, 36:247 – 255, 2014.

[7] J. G. Kassakian and T. M. Jahns. Evolving and emerging applications of power electronics in systems. *IEEE Journal of Emerging and Selected Topics in Power Electronics*, 1(2):47–58, June 2013.

[8] Qobad Shafiee Hassan Bevrani and Hêmin Golpîra. Frequency stability and control in smart grids. *IEEE smartgrid*, 2019. https://smartgrid.ieee.org/newsletters/september-2019/frequency-stability-and-control-in-smart-grids.

[9] M. A. Sofla and L. Wang. Control of dc-dc bidirectional converters for interfacing batteries in microgrids. In *2011 IEEE/PES Power Systems Conference and Exposition*, pages 1–6, 2011.

[10] S. Golestan, M. Monfared, F. D. Freijedo, and J. M. Guerrero. Advantages and challenges of a type-3 pll. *IEEE Transactions on Power Electronics*, 28(11):4985–4997, Nov 2013.

[11] M. Hernandez-Gomez, R. Ortega, F. Lamnabhi-Lagarrigue, and G. Escobar. Adaptive pi stabilization of switched power converters. *IEEE Transactions on Control Systems Technology*, 18(3):688–698, May 2010.

[12] N. Jaalam, N.A. Rahim, A.H.A. Bakar, ChiaKwang Tan, and Ahmed M.A. Haidar. A comprehensive review of synchronization methods for grid-connected converters of renewable energy source. *Renewable and Sustainable Energy Reviews*, 59:1471 – 1481, 2016.

[13] M. JASINSKI M. BOBROWSKA-RAFAL, K. RAFAL and M.P. KAZMIERKOWSKI. Grid synchronization and symmetrical components extraction with pll algorithm for grid connected power electronic converters – a review. *BULLETIN OF THE POLISH ACADEMY OF SCIENCES TECHNICAL SCIENCES, Vol. 59, No. 4*, pages 485–497, 2011.

[14] Salvatore D'Arco, Jon Are Suul, and Olav B. Fosso. Small-signal modeling and parametric sensitivity of a virtual synchronous machine in islanded operation. *International Journal of Electrical Power Energy Systems*, 72:3 – 15, 2015. The Special Issue for 18th Power Systems Computation Conference.

[15] J.-J. E. Slotine and W. Li. *Applied Nonlinear Control, 1s ed*. Prentice Hall, Upple Saddle River, New Jersey, 1991.

[16] Hassan K. Khalil. *Nonlinear Systems Third Edition*. Prentice Hall, Upper Saddle River, New Jersey, USA, 2002.

[17] M. Perez, R. Ortega, and J. R. Espinoza. Passivity-based pi control of switched power converters. *IEEE Transactions on Control Systems Technology*, 12(6), 2004.

[18] Gerardo Escobar, Arjan J. van der Schaft, and Romeo Ortega. A hamiltonian viewpoint in the modeling of switching power converters. *Automatica*, 35(3):445 – 452, 1999.

[19] S. Teimourzadeh, F. Aminifar, and M. Shahidehpour. Contingency-constrained optimal placement of micro-pmus and smart meters in microgrids. *IEEE Transactions on Smart Grid*, 10(2):1889–1897, 2019.

[20] A. Shahsavari, A. Sadeghi-Mobarakeh, E. M. Stewart, E. Cortez, L. Alvarez, F. Megala, and H. Mohsenian-Rad. Distribution grid reliability versus regulation market efficiency: An analysis based on micro-pmu data. *IEEE Transactions on Smart Grid*, 8(6):2916–2925, 2017.

[21] F. Zichao, L. Wenhua, and S. Qiang. A unified switching model for vsc validated by igcts and igbts. In *APEC 07 - Twenty-Second Annual IEEE Applied Power Electronics Conference and Exposition*, pages 1485–1488, 2007.

[22] N. Ahmed, L. Ängquist, S. Norrga, A. Antonopoulos, L. Harnefors, and H. Nee. A computationally efficient continuous model for the modular multilevel converter. *IEEE Journal of Emerging and Selected Topics in Power Electronics*, 2(4):1139–1148, 2014.

[23] Yonghua Song Xi-Fan Wang and Malcolm Irving. *Modern Power Systems Analysis*. Springer Science+Business Media, New York, USA, 2008, ch.8, pp. 489-534.

[24] N. Kroutikova, C. A. Hernandez-Aramburo, and T. C. Green. State-space model of grid-connected inverters under current control mode. *IET Electric Power Applications*, 1(3):329–338, 2007.

[25] Xi-Fan Wang. *Modern Power Systems Analysis*. Springer-Verlag US, Boston, MA, 2008.

[26] Hadi Saadat. *Power System Analysis Third Edition*. PSA publishing, United States of America, 2010.

[27] Jonas Persson. Using linear analysis to find eigenvalues and eigenvectors in power systems. 01 2002.

[28] Prabha Kundur. *Power System Stability and Control*. McGraw-Hill, New York, USA, 1994.

[29] Nima Monshizadeh, Pooya Monshizadeh, Romeo Ortega, and Arjan [van der Schaft]. Conditions on shifted passivity of port-hamiltonian systems. *Systems Control Letters*, 123:55 – 61, 2019.

Appendix A

Validation of Port Hamiltonian representation used in this work

The port Hamiltonian representation in [11] needed to be extended and validated. In this chapter the validation is shown.

$$\dot{x} = (J_0 + \sum_{i=1}^{m} J_i u_i - R)\nabla H(x) + (G_o + \sum_{i=1}^{m} G_i u_i)E + G_\omega u$$
$$\dot{x} = (J_0 - R)\nabla H(x) + \sum_{i=1}^{m} J_i Q x u_i + G_0 E + \sum_{i=1}^{m} J_i G_i E u_i + \sum_{i=1}^{m} J_i G_\omega u_i$$
$$\dot{x} = (J_0 - R)\nabla H(x) + G_0 E + \underbrace{([J_1 Q x + G_1 E, ..., J_m Q x + G_m E] + G_\omega)}_{G_N(x)} u$$

Get on incremental mode where:

$$\tilde{x} = x - x^*$$
$$\tilde{u} = u - u^* \rightarrow u = \tilde{u} - u^*$$

$$\dot{x} = (J_0 - R)\nabla H(x) + \underbrace{G_0 E}_{Constant} + G_N(x)u$$
$$-0 = (J_0 - R)\nabla H(x^*) + \underbrace{G_0 E}_{Constant} + G_N(x^*)u$$
$$= \dot{\tilde{x}} = (J_0 - R)\underbrace{Q(x - x^*)}_{\nabla V(x)} + G_N(x)(\tilde{u} + \tilde{u^*}) - GN(x^*)u^*$$

$$\dot{\tilde{x}} = (J_0 - R)\nabla V(x) + G_N(x)\tilde{u} + [G_N(x) - G_N(x^*)]u^*$$

And now extract $([G_N(x) - G_N(x^*)])u^*$, locate and remove the constants.

$$([(J_1 Qx + \underbrace{G_1 E}_{Constant}, ..., J_m Q_x + \underbrace{G_m E}_{Constant}] + \underbrace{G_\omega}_{Constant}) -$$
$$([J_1 Qx^* + \underbrace{G_1 E}_{Constant}, ..., J_m Qx^* + \underbrace{G_m E}_{Constant}] + \underbrace{G_\omega}_{Constant})])u^*$$

Simplify the term:

$$[J_1 Q(x - x^*), ..., J_m Q(x - x^*)]u^*$$
$$\Downarrow$$
$$\sum_{i=1}^{m} J_i u_i^* \nabla V(x)$$

And now included in the original model:

$$\dot{\tilde{x}} = (J_0 + \sum_{i=1}^{m} -R)\nabla V(x) + G_N(x)\tilde{u}$$
$$V(x) = \frac{1}{2} \cdot \tilde{x}^T \mathcal{Q} \tilde{x}$$
$$\dot{V} = \nabla^T V \dot{\tilde{x}}$$
$$\dot{V} = \underbrace{-\nabla^T V(x) R \nabla V(x)}_{pseudodissipation} + \underbrace{\nabla^T V(x) G_N(x)}_{y^T} \tilde{u}$$
$$\dot{V} \leq y^T \tilde{u}$$

Hence the extension is proved and the converter can be stabilized with a PI controller.

Appendix B

Equations for Port Hamiltonian

B.1 Original

This appendix illustrates the different matrices used for designing the different PLLs. Each section is divided into two subsections, where the first section concerns the port-Hamiltonian representation and the second subsection shows the matrices used for the passivity controller design.

B.1.1 Port-Hamiltonian

$$\dot{x} = \begin{bmatrix} \phi_{v,d} & \phi_{v,q} & q_{f,d} & q_{f,q} & \phi_{g,d} & \phi_{g,q} \end{bmatrix}^\top \tag{B.1}$$

$$J_0 = \begin{bmatrix} 0 & L_f\omega & -1 & 0 & 0 & 0 \\ -L_f\omega & 0 & 0 & -1 & 0 & 0 \\ 1 & 0 & 0 & C\omega & -1 & 0 \\ 0 & 1 & C\omega & 0 & 0 & -1 \\ 0 & 0 & 1 & 0 & 0 & L_g\omega \\ 0 & 0 & 0 & 1 & -L_g\omega & 0 \end{bmatrix} \tag{B.2}$$

$$R = \begin{bmatrix} R_f & 0 & 0 & 0 & 0 & 0 \\ 0 & R_f & 0 & 0 & 0 & 0 \\ 0 & 0 & 0 & 0 & 0 & 0 \\ 0 & 0 & 0 & 0 & 0 & 0 \\ 0 & 0 & 0 & 0 & R_g & 0 \\ 0 & 0 & 0 & 0 & 0 & R_g \end{bmatrix} \tag{B.3}$$

$$G_0 = \begin{bmatrix} 0 & 0 & 0 & 0 \\ 0 & 0 & 0 & 0 \\ 0 & 0 & 0 & 0 \\ 0 & 0 & 0 & 0 \\ 0 & -1 & 0 & 0 \\ 0 & 0 & -1 & 0 \end{bmatrix} \tag{B.4}$$

$$G_1 = \begin{bmatrix} 1 & 0 & 0 & 0 \\ 0 & 0 & 0 & 0 \\ 0 & 0 & 0 & 0 \\ 0 & 0 & 0 & 0 \\ 0 & 0 & 0 & 0 \\ 0 & 0 & 0 & 0 \end{bmatrix} \tag{B.5}$$

$$G_2 = \begin{bmatrix} 0 & 0 & 0 & 0 \\ 1 & 0 & 0 & 0 \\ 0 & 0 & 0 & 0 \\ 0 & 0 & 0 & 0 \\ 0 & 0 & 0 & 0 \\ 0 & 0 & 0 & 0 \end{bmatrix} \tag{B.6}$$

$$E = \begin{bmatrix} V_{DC} & V_{g,d} & V_{g,q} & \omega_g \end{bmatrix}^\top \tag{B.7}$$

$$u = \begin{bmatrix} m_d \\ m_q \end{bmatrix} \tag{B.8}$$

B.1.2 Passive Output

$$Q = \begin{bmatrix} \frac{1}{L_f} & 0 & 0 & 0 & 0 & 0 \\ 0 & \frac{1}{L_f} & 0 & 0 & 0 & 0 \\ 0 & 0 & \frac{1}{C} & 0 & 0 & 0 \\ 0 & 0 & 0 & \frac{1}{C} & 0 & 0 \\ 0 & 0 & 0 & 0 & \frac{1}{L_g} & 0 \\ 0 & 0 & 0 & 0 & 0 & \frac{1}{L_g} \end{bmatrix} \tag{B.9}$$

$$\tilde{x} = \begin{bmatrix} \phi_{v,d} - \phi^*_{v,d} \\ \phi_{v,q} - \phi^*_{v,q} \\ q_{f,d} - q^*_{f,d} \\ q_{f,q} - q^*_{f,q} \\ \phi_{g,d} - \phi^*_{g,d} \\ \phi_{g,q} - \phi^*_{g,q} \end{bmatrix}^\top \tag{B.10}$$

$$G_N(x) = \begin{bmatrix} V_{DC} & 0 \\ 0 & V_{DC} \\ 0 & 0 \\ 0 & 0 \\ 0 & 0 \\ 0 & 0 \end{bmatrix} \tag{B.11}$$

A hyperlink in 3.2 is included in order to return to Chapter 3.2.

B.2 Alternative 0

B.2.1 Port-Hamiltonian

$$\dot{x} = \begin{bmatrix} \phi_{v,d} & \phi_{v,q} & q_{f,d} & q_{f,q} & \phi_{g,d} & \phi_{g,q} & \delta \end{bmatrix} \tag{B.12}$$

$$J_0 = \begin{bmatrix} 0 & 0 & -1 & 0 & 0 & 0 & 0 \\ 0 & 0 & 0 & -1 & 0 & 0 & 0 \\ 1 & -0 & 0 & C\omega_g & -1 & 0 & 0 \\ 0 & 1 & -C\omega_g & 0 & 0 & -1 & 0 \\ 0 & 0 & 1 & 0 & 0 & L_g\omega_g & 0 \\ 0 & 0 & 0 & 1 & -L_g\omega_g & 0 & 0 \\ 0 & 0 & 0 & 0 & 0 & 0 & 0 \end{bmatrix} \tag{B.13}$$

$$J_1 = \begin{bmatrix} 0 & L_f & 0 & 0 & 0 & 0 & 0 \\ -Lf & 0 & 0 & 0 & 0 & 0 & 0 \\ 0 & 0 & 0 & 0 & 0 & 0 & 0 \\ 0 & 0 & 0 & 0 & 0 & 0 & 0 \\ 0 & 0 & 0 & 0 & 0 & 0 & 0 \\ 0 & 0 & 0 & 0 & 0 & 0 & 0 \\ 0 & 0 & 0 & 0 & 0 & 0 & 0 \end{bmatrix} \tag{B.14}$$

$$R = \begin{bmatrix} R_f & 0 & 0 & 0 & 0 & 0 & 0 \\ 0 & R_f & 0 & 0 & 0 & 0 & 0 \\ 0 & 0 & 0 & 0 & 0 & 0 & 0 \\ 0 & 0 & 0 & 0 & 0 & 0 & 0 \\ 0 & 0 & 0 & 0 & R_g & 0 & 0 \\ 0 & 0 & 0 & 0 & 0 & R_g & 0 \\ 0 & 0 & 0 & 0 & 0 & 0 & 0 \end{bmatrix} \tag{B.15}$$

$$G_0 = \begin{bmatrix} 0 & 0 & 0 & 0 \\ 0 & 0 & 0 & 0 \\ 0 & 0 & 0 & 0 \\ 0 & 0 & 0 & 0 \\ 0 & -1 & 0 & 0 \\ 0 & 0 & -1 & 0 \\ 0 & 0 & 0 & -1 \end{bmatrix} \tag{B.16}$$

$$G_1 = \begin{bmatrix} 1 & 0 & 0 & 0 \\ 0 & 0 & 0 & 0 \\ 0 & 0 & 0 & 0 \\ 0 & 0 & 0 & 0 \\ 0 & 0 & 0 & 0 \\ 0 & 0 & 0 & 0 \\ 0 & 0 & 0 & 0 \end{bmatrix} \tag{B.17}$$

$$G_2 = \begin{bmatrix} 0 & 0 & 0 & 0 \\ 1 & 0 & 0 & 0 \\ 0 & 0 & 0 & 0 \\ 0 & 0 & 0 & 0 \\ 0 & 0 & 0 & 0 \\ 0 & 0 & 0 & 0 \\ 0 & 0 & 0 & 0 \end{bmatrix} \tag{B.18}$$

$$E = \begin{bmatrix} V_{DC} \\ V_{g,d} \\ V_{g,q} \\ \omega_g \end{bmatrix} \tag{B.19}$$

$$u = \begin{bmatrix} \omega_{\text{pll}} \\ m_d \\ m_q \end{bmatrix} \tag{B.20}$$

$$G_\omega = \begin{bmatrix} 0 & 0 & 0 \\ 0 & 0 & 0 \\ 0 & 0 & 0 \\ 0 & 0 & 0 \\ 0 & 0 & 0 \\ 0 & 0 & 0 \\ 1 & 0 & 0 \end{bmatrix} \tag{B.21}$$

B.2.2 Passive output

$$Q = \begin{bmatrix} \frac{1}{L_f} & 0 & 0 & 0 & 0 & 0 & 0 \\ 0 & \frac{1}{L_f} & 0 & 0 & 0 & 0 & 0 \\ 0 & 0 & \frac{1}{C} & 0 & 0 & 0 & 0 \\ 0 & 0 & 0 & \frac{1}{C} & 0 & 0 & 0 \\ 0 & 0 & 0 & 0 & \frac{1}{L_g} & 0 & 0 \\ 0 & 0 & 0 & 0 & 0 & \frac{1}{L_g} & 0 \\ 0 & 0 & 0 & 0 & 0 & 0 & \frac{1}{\tau\delta} \end{bmatrix} \tag{B.22}$$

$$\tilde{x} = \begin{bmatrix} \phi_{v,d} - \phi^*_{v,d} \\ \phi_{v,q} - \phi^*_{v,q} \\ q_{f,d} - q^*_{f,d} \\ q_{f,q} - q^*_{f,q} \\ \phi_{g,d} - \phi^*_{g,d} \\ \phi_{g,q} - \phi^*_{g,q} \end{bmatrix}^\top \tag{B.23}$$

$$G_N(x) = \begin{bmatrix} L_f i_{v,q} & V_{DC} & 0 \\ -L_f i_{v,d} & 0 & V_{DC} \\ 0 & 0 & 0 \\ 0 & 0 & 0 \\ 0 & 0 & 0 \\ 0 & 0 & 0 \\ 1 & 0 & 0 \end{bmatrix} \tag{B.24}$$

A hyperlink in 3.2 is included in order to return to Chapter 3.2.

B.3 Alternative 1

B.3.1 Port-Hamiltonian

$$\dot{x} = \begin{bmatrix} \phi_{v,d} & \phi_{v,q} & q_{v,d} & q_{v,q} & \phi_{g,d} & \phi_{g,q} & \delta \end{bmatrix}^\top \tag{B.25}$$

$$J_0 = \begin{bmatrix} 0 & 0 & -1 & 0 & 0 & 0 & 0 \\ 0 & 0 & & -1 & 0 & 0 & 0 \\ 1 & 0 & 0 & 0 & -1 & 0 & 0 \\ 0 & 1 & 0 & 0 & -0 & -1 & 0 \\ 0 & 0 & 1 & 0 & 0 & L_g\omega_g & 0 \\ 0 & 0 & -0 & 1 & -L_g\omega_g & 0 & 0 \\ 0 & 0 & 0 & 0 & 0 & 0 & 0 \end{bmatrix} \tag{B.26}$$

$$J_1 = \begin{bmatrix} 0 & L_f & 0 & 0 & 0 & 0 & 0 \\ -Lf & 0 & 0 & 0 & 0 & 0 & 0 \\ 0 & 0 & 0 & C & 0 & 0 & 0 \\ 0 & 0 & -C & 0 & 0 & 0 & 0 \\ 0 & 0 & 0 & 0 & 0 & 0 & 0 \\ 0 & 0 & 0 & 0 & 0 & 0 & 0 \\ 0 & 0 & 0 & 0 & 0 & 0 & 0 \end{bmatrix} \tag{B.27}$$

$$R = \begin{bmatrix} R_f & 0 & 0 & 0 & 0 & 0 & 0 \\ 0 & R_f & 0 & 0 & 0 & 0 & 0 \\ 0 & 0 & 0 & 0 & 0 & 0 & 0 \\ 0 & 0 & 0 & 0 & 0 & 0 & 0 \\ 0 & 0 & 0 & 0 & R_g & 0 & 0 \\ 0 & 0 & 0 & 0 & 0 & R_g & 0 \\ 0 & 0 & 0 & 0 & 0 & 0 & 0 \end{bmatrix} \tag{B.28}$$

$$G_0 = \begin{bmatrix} 0 & 0 & 0 & 0 \\ 0 & 0 & 0 & 0 \\ 0 & 0 & 0 & 0 \\ 0 & 0 & 0 & 0 \\ 0 & -1 & 0 & 0 \\ 0 & 0 & -1 & 0 \\ 0 & 0 & 0 & -1 \end{bmatrix} \tag{B.29}$$

$$G_1 = \begin{bmatrix} 1 & 0 & 0 & 0 \\ 0 & 0 & 0 & 0 \\ 0 & 0 & 0 & 0 \\ 0 & 0 & 0 & 0 \\ 0 & 0 & 0 & 0 \\ 0 & 0 & 0 & 0 \\ 0 & 0 & 0 & 0 \end{bmatrix} \tag{B.30}$$

$$G_2 = \begin{bmatrix} 0 & 0 & 0 & 0 \\ 1 & 0 & 0 & 0 \\ 0 & 0 & 0 & 0 \\ 0 & 0 & 0 & 0 \\ 0 & 0 & 0 & 0 \\ 0 & 0 & 0 & 0 \\ 0 & 0 & 0 & 0 \end{bmatrix} \tag{B.31}$$

$$E = \begin{bmatrix} V_{DC} \\ V_{g,d} \\ V_{g,q} \\ \omega_g \end{bmatrix} \tag{B.32}$$

$$u = \begin{bmatrix} \omega_{\text{pll}} \\ m_d \\ m_q \end{bmatrix} \tag{B.33}$$

$$G_\omega = \begin{bmatrix} 0 & 0 & 0 \\ 0 & 0 & 0 \\ 0 & 0 & 0 \\ 0 & 0 & 0 \\ 0 & 0 & 0 \\ 0 & 0 & 0 \\ 1 & 0 & 0 \end{bmatrix} \tag{B.34}$$

B.3.2 Passive Output

$$Q = \begin{bmatrix} \frac{1}{L_f} & 0 & 0 & 0 & 0 & 0 & 0 \\ 0 & \frac{1}{L_f} & 0 & 0 & 0 & 0 & 0 \\ 0 & 0 & \frac{1}{C} & 0 & 0 & 0 & 0 \\ 0 & 0 & 0 & \frac{1}{C} & 0 & 0 & 0 \\ 0 & 0 & 0 & 0 & \frac{1}{L_g} & 0 & 0 \\ 0 & 0 & 0 & 0 & 0 & \frac{1}{L_g} & 0 \\ 0 & 0 & 0 & 0 & 0 & 0 & \frac{1}{\tau\delta} \end{bmatrix} \tag{B.35}$$

$$\tilde{x} = \begin{bmatrix} \phi_{v,d} - \phi^*_{v,d} \\ \phi_{v,q} - \phi^*_{v,q} \\ q_{f,d} - q^*_{f,d} \\ q_{f,q} - q^*_{f,q} \\ \phi_{g,d} - \phi^*_{g,d} \\ \phi_{g,q} - \phi^*_{g,q} \end{bmatrix}^\top \tag{B.36}$$

$$G_N(x) = \begin{bmatrix} L_f i_{v,q} & V_{DC} & 0 \\ -L_f i_{v,d} & 0 & V_{DC} \\ C v_{f,q} & 0 & 0 \\ -C v_{f,d} & 0 & 0 \\ 0 & 0 & 0 \\ 0 & 0 & 0 \\ 1 & 0 & 0 \end{bmatrix} \tag{B.37}$$

A hyperlink in 3.2 is included in order to return to Chapter 3.2.

B.4 Alternative 2

B.4.1 Port-Hamiltonian

$$\dot{x} = \begin{bmatrix} \phi_{v,d} & \phi_{v,q} & q_{v,d} & q_{v,q} & \phi_{g,d} & \phi_{g,q} & \dot{\delta} \end{bmatrix}^\top \tag{B.38}$$

$$J_0 = \begin{bmatrix} 0 & 0 & -1 & 0 & 0 & 0 & 0 \\ 0 & 0 & 0 & -1 & 0 & 0 & 0 \\ 1 & 0 & 0 & 0 & -1 & 0 & 0 \\ 0 & 1 & 0 & 0 & 0 & -1 & 0 \\ 0 & 0 & 1 & 0 & 0 & 0 & 0 \\ 0 & 0 & 0 & 1 & 0 & 0 & 0 \\ 0 & 0 & 0 & 0 & 0 & 0 & 0 \end{bmatrix} \tag{B.39}$$

$$J_1 = \begin{bmatrix} 0 & L_f & 0 & 0 & 0 & 0 & 0 \\ -Lf & 0 & 0 & 0 & 0 & 0 & 0 \\ 0 & 0 & 0 & C & 0 & 0 & 0 \\ 0 & 0 & -C & 0 & 0 & 0 & 0 \\ 0 & 0 & 0 & 0 & 0 & L_g & 0 \\ 0 & 0 & 0 & 0 & -L_g & 0 & 0 \\ 0 & 0 & 0 & 0 & 0 & 0 & 0 \end{bmatrix} \tag{B.40}$$

$$R = \begin{bmatrix} R_f & 0 & 0 & 0 & 0 & 0 & 0 \\ 0 & R_f & 0 & 0 & 0 & 0 & 0 \\ 0 & 0 & 0 & 0 & 0 & 0 & 0 \\ 0 & 0 & 0 & 0 & 0 & 0 & 0 \\ 0 & 0 & 0 & 0 & R_g & 0 & 0 \\ 0 & 0 & 0 & 0 & 0 & R_g & 0 \\ 0 & 0 & 0 & 0 & 0 & 0 & 0 \end{bmatrix} \tag{B.41}$$

$$G_0 = \begin{bmatrix} 0 & 0 & 0 & 0 \\ 0 & 0 & 0 & 0 \\ 0 & 0 & 0 & 0 \\ 0 & 0 & 0 & 0 \\ 0 & -1 & -0 & 0 \\ 0 & 0 & -1 & 0 \\ 0 & 0 & 0 & -1 \end{bmatrix} \tag{B.42}$$

$$G_1 = \begin{bmatrix} 1 & 0 & 0 & 0 \\ 0 & 0 & 0 & 0 \\ 0 & 0 & 0 & 0 \\ 0 & 0 & 0 & 0 \\ 0 & 0 & 0 & 0 \\ 0 & 0 & 0 & 0 \\ 0 & 0 & 0 & 0 \end{bmatrix} \tag{B.43}$$

$$G_2 = \begin{bmatrix} 0 & 0 & 0 & 0 \\ 1 & 0 & 0 & 0 \\ 0 & 0 & 0 & 0 \\ 0 & 0 & 0 & 0 \\ 0 & 0 & 0 & 0 \\ 0 & 0 & 0 & 0 \\ 0 & 0 & 0 & 0 \end{bmatrix} \tag{B.44}$$

$$E = \begin{bmatrix} V_{DC} \\ V_{g,d} \\ V_{g,q} \\ \omega_g \end{bmatrix} \tag{B.45}$$

$$u = \begin{bmatrix} \omega_{\text{pll}} \\ m_d \\ m_q \end{bmatrix} \tag{B.46}$$

$$G_\omega = \begin{bmatrix} 0 & 0 & 0 \\ 0 & 0 & 0 \\ 0 & 0 & 0 \\ 0 & 0 & 0 \\ 0 & 0 & 0 \\ 0 & 0 & 0 \\ 1 & 0 & 0 \end{bmatrix} \tag{B.47}$$

B.4.2 Passive Output

$$Q = \begin{bmatrix} \frac{1}{L_f} & 0 & 0 & 0 & 0 & 0 & 0 \\ 0 & \frac{1}{L_f} & 0 & 0 & 0 & 0 & 0 \\ 0 & 0 & \frac{1}{C} & 0 & 0 & 0 & 0 \\ 0 & 0 & 0 & \frac{1}{C} & 0 & 0 & 0 \\ 0 & 0 & 0 & 0 & \frac{1}{L_g} & 0 & 0 \\ 0 & 0 & 0 & 0 & 0 & \frac{1}{L_g} & 0 \\ 0 & 0 & 0 & 0 & 0 & 0 & \frac{1}{\tau\delta} \end{bmatrix} \tag{B.48}$$

$$\tilde{x} = \begin{bmatrix} \phi_{v,d} - \phi^*_{v,d} \\ \phi_{v,q} - \phi^*_{v,q} \\ q_{v,d} - q^*_{v,d} \\ q_{f,q} - q^*_{f,q} \\ \phi_{g,d} - \phi^*_{g,d} \\ \phi_{g,q} - \phi^*_{g,q} \\ \delta - \delta^* \end{bmatrix}^\top \tag{B.49}$$

$$G_N(x) = \begin{bmatrix} L_f i_{v,q} & V_{DC} & 0 \\ -L_f i_{v,d} & 0 & V_{DC} \\ C V_{f,q} & 0 & 0 \\ -C V_{f,d} & 0 & 0 \\ L_g i_{g,q} & 0 & 0 \\ -L_g i_{g,d} & 0 & 0 \\ 1 & 0 & 0 \end{bmatrix} \tag{B.50}$$

A hyperlink in 3.2 is included in order to return to Chapter 3.2.

Appendix C

Performance Without Knowing δ

C.1 Original PLL

Table C.1: The calculated steady state values when δ is estimated. Original model

State	Value	Unit
$i_{v,d}$	10	[A]
$i_{v,q}$	0	[A]
$v_{f,d}$	328.2028	[V]
$v_{f,q}$	0	[V]
$i_{g,d}$	7.0464	[A]
$i_{g,q}$	-13.2821	[A]
δ	-0.7889	[-]
A	0.0051	[-]
B	0.2186	[-]
C	0.0054	[-]

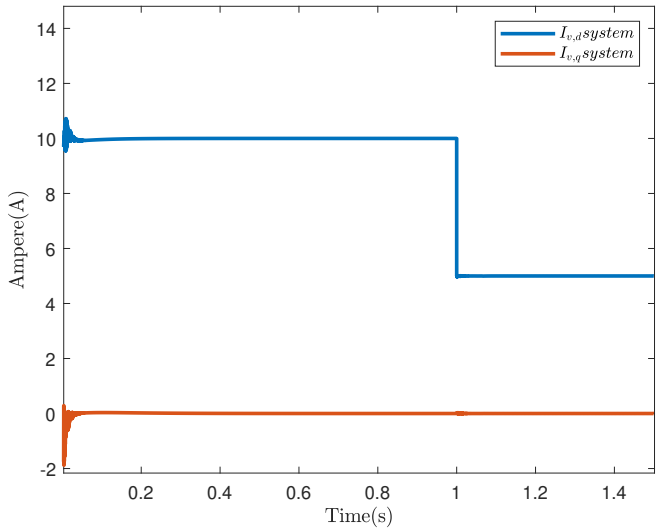

Figure C.1: Converter current in SRF when delta is estimated. Original model

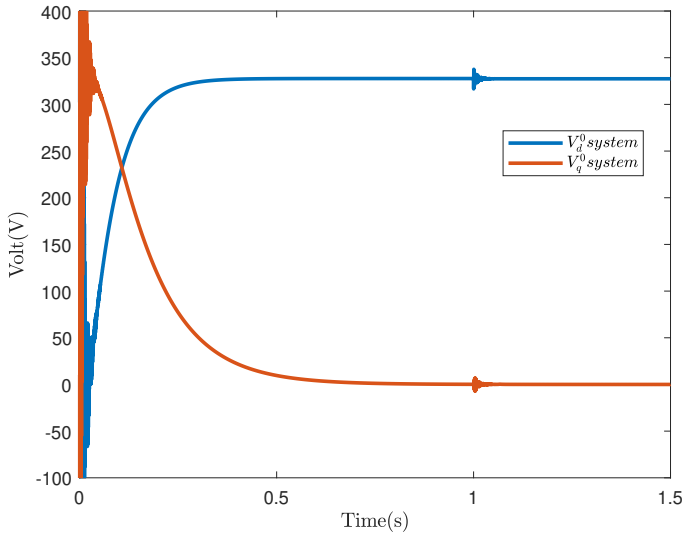

Figure C.2: Voltage across the capacitor in SRF when delta is estimated. Original model

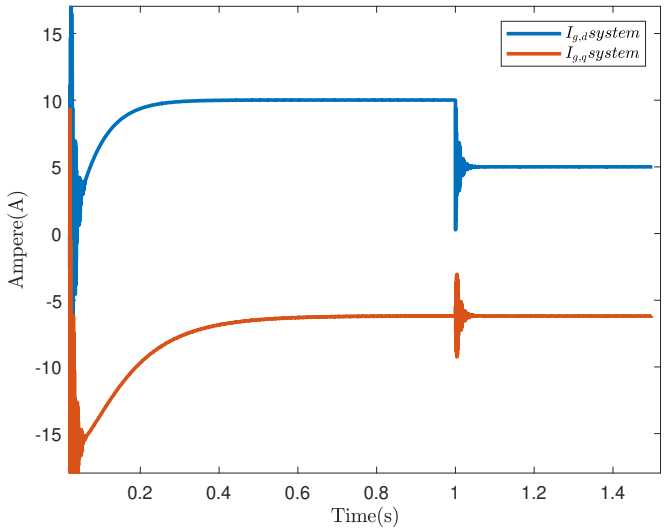

Figure C.3: Grid current in SRF when delta is estimated. Original model

C.2 Alternative 0

Table C.2: The calculated steady state values when δ is estimated. Alternative 0

State	Value	Unit
$i_{v,d}$	10	[A]
$i_{v,q}$	0	[A]
$V_{f,d}$	328.2028	[V]
$v_{f,q}$	0	[V]
$i_{g,d}$	7.0464	[A]
$i_{g,q}$	-13.2821	[A]
δ	-0.7889	[-]
A	0.001	[-]
B	-0.0437	[-]
C	0.0011	[-]

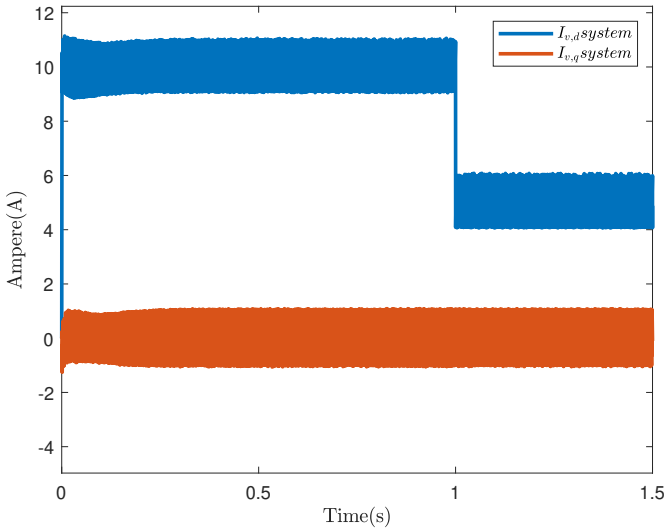

Figure C.4: Converter current in SRF when delta is estimated. Alternative 0

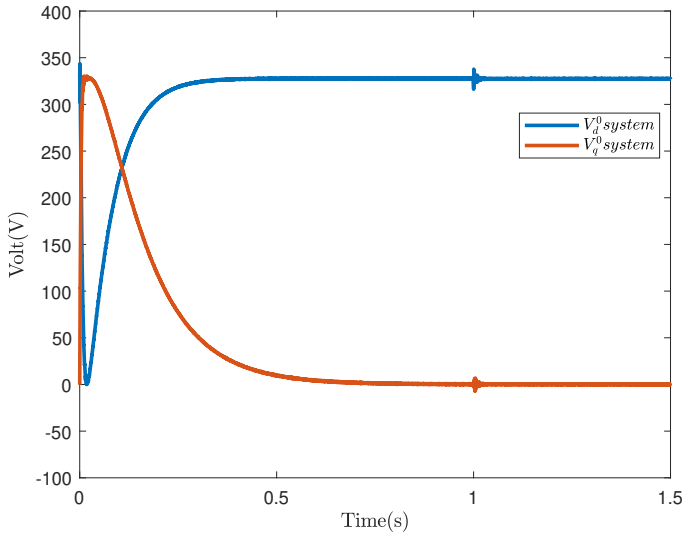

Figure C.5: Voltage across the capacitor in SRF when delta is estimated. Alternative 0

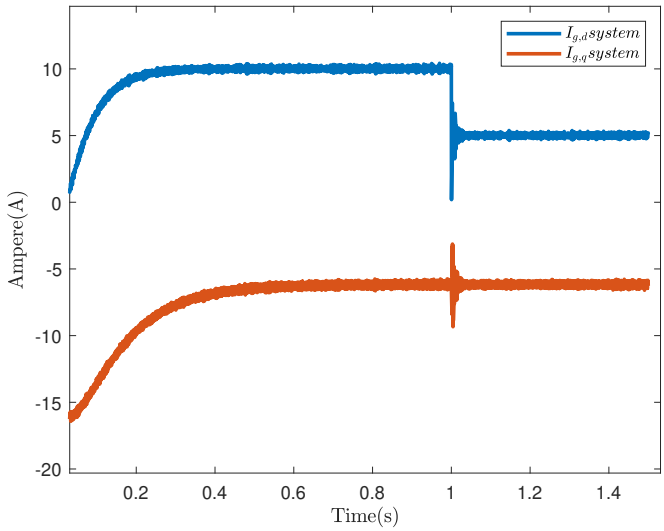

Figure C.6: Grid current in SRF when delta is estimated. Alternative 0

C.3 Alternative 1

Table C.3: The calculated steady state values when δ is estimated. Alternative 1.

State	Value	Unit
$i_{v,d}$	10	[A]
$i_{v,q}$	0	[A]
$v_{f,d}$	327.6802	[V]
$v_{f,q}$	0	[V]
$i_{g,d}$	10.012	[A]
$i_{g,q}$	-6.1572	[A]
δ	-0.0019	[-]
A	0.0072	[-]
B	0.2186	[-]
C	0.0003	[-]

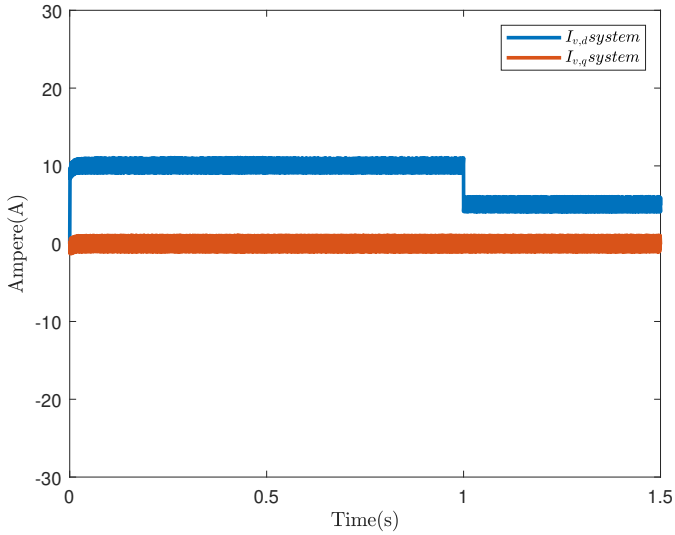

Figure C.7: Converter current in SRF when delta is estimated. Alternative 1

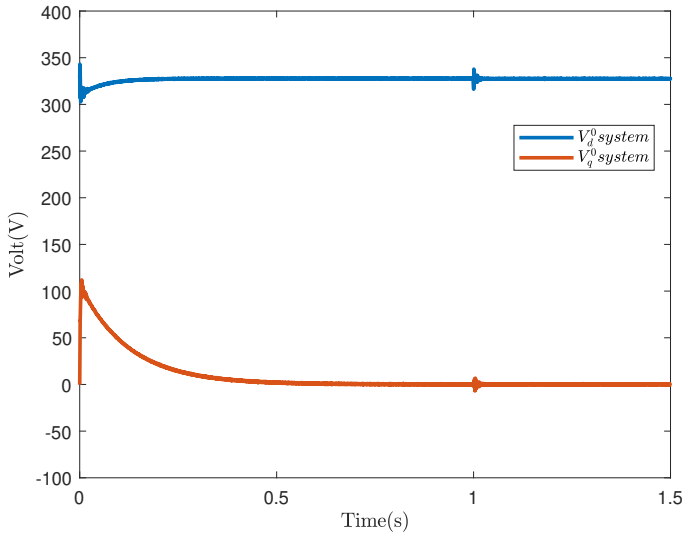

Figure C.8: Voltage across the capacitor in SRF when delta is estimated. Alternative 1

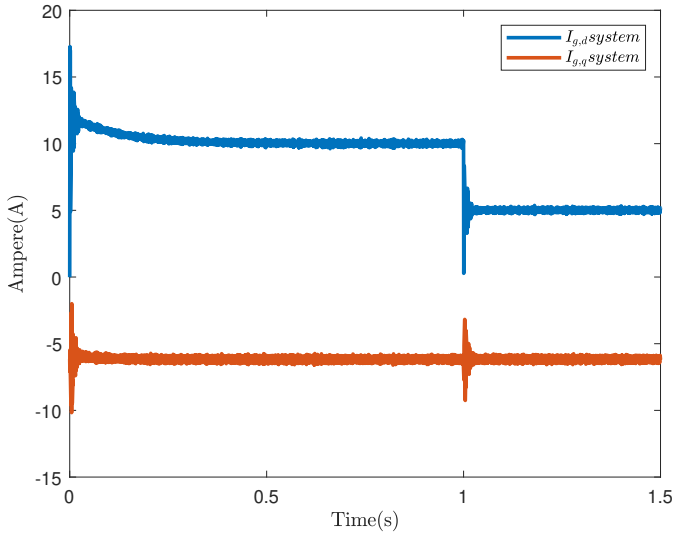

Figure C.9: Grid current in SRF when delta is estimated. Alternative 1

C.4 Alternative 2

Table C.4: The calculated steady state values when δ is estimated. Alternative 2.

State	Value	Unit
$i_{v,d}$	10	[A]
$i_{v,q}$	0	[A]
$v_{f,d}$	327.0992	[V]
$v_{f,q}$	-0.988	[V]
$i_{g,d}$	10	[A]
$i_{g,q}$	-0.0062	[A]
δ	-0.0001	[-]
A	0.0072	[-]
B	0.2186	[-]
C	0.0002	[-]

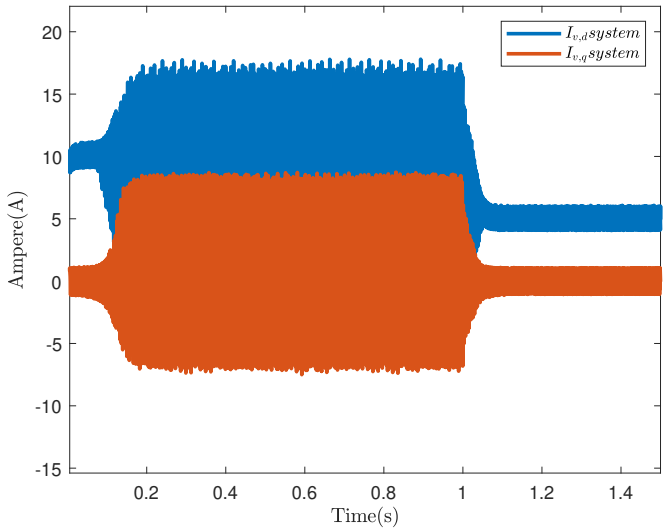

Figure C.10: Converter current in SRF when delta is estimated. Alternative 2

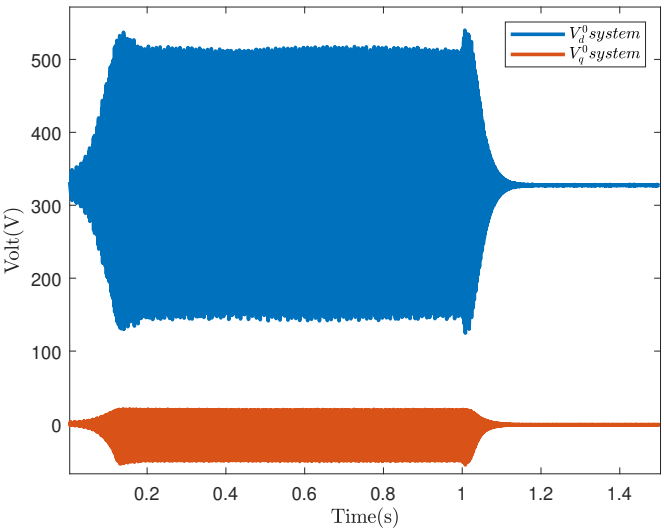

Figure C.11: Voltage across the capacitor in SRF when delta is estimated. Alternative 2

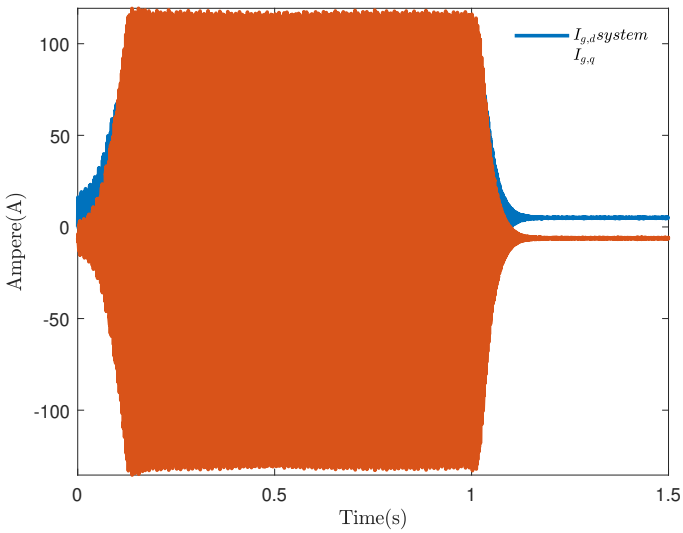

Figure C.12: Grid current in SRF when delta is estimated. Alternative 2

Appendix D

Eigenvalues and Participation factor when δ is known

D.1 Orginal

Table D.1: Eigenvalues related to the original PLL.

Eigenvalue Nr.	Real	Imaginary
1	-6.41E+07	314.16i
2	-6.41E+07	-314.16i
3	-83.367	7767.3i
4	-83.367	-7767.3i
5	-83.367	7138.9i
6	-83.367	-7138.9i
7	-130	0.00068689i
8	-130	- 0.00068689i
9	-171.63	0i
10	-8.3728	0i

Table D.2: The participation factors for the different eigenvalues related to the model including the original PLL.

	Eigenvalue Nr.									
	1	2	3	4	5	6	7	8	9	10
$i_{v,d}$	0.5	0.5	0	0	0	0	0	0	0	0
$i_{v,q}$	0.5	0.5	0	0	0	0	0	0	0	0
$v_{f,d}$	0	0	0.25	0.25	0.25	0.25	0	0	0	0
$v_{f,q}$	0	0	0.25	0.25	0.25	0.25	0	0	0	0
$i_{g,d}$	0	0	0.25	0.25	0.25	0.25	0	0	0	0
$i_{g,q}$	0	0	0.25	0.25	0.25	0.25	0	0	0	0
δ	0	0	0	0	0	0	0	0	0.9535	0.0465
A	0	0	0	0	0	0	0.5	0.5	0	0
B	0	0	0	0	0	0	0	0	0.0465	0.9535
C	0	0	0	0	0	0	0.5	0.5	0	0

D.2 Alternative 0

Table D.3: Eigenvalues related to the alternative 0 model.

Eigenvalue Nr.	Real	Imaginary
1	-6.41E+07	+ 52.589i
2	-6.41E+07	- 52.589i
3	-83.367	+ 7767.3i
4	-83.367	- 7767.3i
5	-83.367	+ 7138.9i
6	-83.367	- 7138.9i
7	-650.01	+ 0i
8	-649.99	+ 0i
9	-171.63	+ 0i
10	-8.3728	+ 0i

Table D.4: The participation factors for the different eigenvalues related to the alternative 0 model.

	Eigenvalue Nr									
	1	2	3	4	5	6	7	8	9	10
$i_{v,d}$	0.5	0.5	0	0	0	0	0	0	0	0
$i_{v,q}$	0.5	0.5	0	0	0	0	0	0	0	0
$v_{f,d}$	0	0	0.25	0.25	0.25	0.25	0	0	0	0
$v_{f,q}$	0	0	0.25	0.25	0.25	0.25	0	0	0	0
$i_{g,d}$	0	0	0.25	0.25	0.25	0.25	0	0	0	0
$i_{g,q}$	0	0	0.25	0.25	0.25	0.25	0	0	0	0
δ	0	0	0	0	0	0	0	0	0.9535	0.0465
A	0	0	0	0	0	0	0.9991	0.0009	0	0
B	0	0	0	0	0	0	0	0	0.0465	0.9535
C	0	0	0	0	0	0	0.0009	0.9991	0	0

D.3 Alternative 1

Table D.5: Eigenvalues related to the alternative 1 model.

Eigenvalue Nr.	Real	Imaginary
1	-6.41E+07	+ 312.27i
2	-6.41E+07	- 312.27i
3	-175.25	+ 7442.1i
4	-175.25	- 7442.1i
5	-1124.2	+ 7571.6i
6	-1124.2	- 7571.6i
7	933.71	+ 0i
8	-130	+ 0.00039484i
9	-130	- 0.00039484i
10	-7.9192	+ 0i

Table D.6: The participation factors for the different eigenvalues related to the alternative 1 model.

	Eigenvalue Number									
	1	2	3	4	5	6	7	8	9	10
$i_{v,d}$	0.5	0.5	0	0	0	0	0	0	0	0
$i_{v,q}$	0.5	0.5	0	0	0	0	0	0	0	0
$v_{f,d}$	0	0	0.4568	0.4568	0.0386	0.0386	0.0001	0	0	0
$v_{f,q}$	0	0	0.0399	0.0399	0.4327	0.4327	0.0198	0	0	0
$i_{g,d}$	0	0	0.4577	0.4577	0.0394	0.0394	0	0	0	0
$i_{g,q}$	0	0	0.0393	0.0393	0.4257	0.4257	0.0439	0	0	0
δ	0	0	0.0062	0.0062	0.0634	0.0634	0.9285	0	0	0.008
A	0	0	0	0	0	0	0	0.5	0.5	0
B	0	0	0	0	0.0001	0.0001	0.0077	0	0	0.992
C	0	0	0	0	0	0	0	0.5	0.5	0

D.4 Alternative 2

Table D.7: Eigenvalues related to the alternative 2 model.

Eigenvalue Nr.	Real	Imaginary
1	-6.41E+07	+ 312.27i
2	-6.41E+07	- 312.27i
3	-82.392	+ 7459.3i
4	-82.392	- 7459.3i
5	-8736.8	+ 0i
6	6238.1	+ 0i
7	996.93	+ 0i
8	-130	+ 0.00033762i
9	-130	- 0.00033762i
10	-7.9188	+ 0i

Table D.8: The participation factors for the different eigenvalues related to the alternative 2 model.

	Eigenvalue Number									
	1	2	3	4	5	6	7	8	9	10
$i_{v,d}$	0.5	0.5	0	0	0	0	0	0	0	0
$i_{v,q}$	0.5	0.5	0	0	0	0	0	0	0	0
$v_{f,d}$	0	0	0.4998	0.4998	0.0001	0.0001	0.0001	0	0	0
$v_{f,q}$	0	0	0.0001	0.0001	0.4989	0.4177	0.0136	0	0	0
$i_{g,d}$	0	0	0.4998	0.4998	0.0001	0.0001	0.0001	0	0	0
$i_{g,q}$	0	0	0.0001	0.0001	0.4438	0.4867	0.0405	0	0	0
δ	0	0	0.0001	0.0001	0.057	0.0951	0.9382	0	0	0.008
A	0	0	0	0	0	0	0	0.5	0.5	0
B	0	0	0	0	0.0001	0.0002	0.0075	0	0	0.992
C	0	0	0	0	0	0	0	0.5	0.5	0

D.4.1 On the stability results

Even though these are only considered as indicative results, it can be seen from the results that with respect to the eigenvalues, the traditional model as well as the model including the alternative 0 PLL are stable. Which leaves the alternative 1 and alternative 2 model unstable. Eigenvalue 7 in alternative 1 is unstable. Even though δ is a known parameter in the calculations, the unstable eigenvalue has 92 % participation factor of δ. While the remaining percentages are mainly related to $i_{g,q}$ and $v_{f,q}$.
For the alternative 2 model, however, the eigenvalue 6 and 7 are unstable. Together with the alternative 1 model, eigenvalue 7 are mainly related to δ (94 %), $i_{g,q}$ (4 %) and $v_{f,q}$ (1,4 %). The same states do also have the highest participating factors of eigenvalue 6, whereas $i_{g,q}$ (49 %), $v_{f,q}$ (42 %) and δ (9 %).

In Appendix E the eigenvalues and the participation factor for the systems including the estimation of δ is shown. What slightly differ these models from the models when δ is known, are the participation factors of the different states. Implying that the estimation of δ is somewhat sufficient. Whereas most of the performance simulations substantiates.

Appendix E

Eigenvalues and Participation Factor when δ is estimated

E.1 Original

Table E.1: The eigenvalues of the model including the original PLL when δ is estimated.

Eigenvalue Nr.	Real	Imaginary
1	-6.41E+07	+ 313.81i
2	-6.41E+07	- 313.81i
3	-83.305	+ 7770.2i
4	-83.305	- 7770.2i
5	-83.285	+ 7142.1i
6	-83.285	- 7142.1i
7	-130	+ 0.00065229i
8	-130	- 0.00065229i
9	-0.14469	+ 1.4778i
10	-0.14469	- 1.4778i

Table E.2: The participation factors related to the eigenvalues in Table E.1.

	Eigenvalue Number									
	1	2	3	4	5	6	7	8	9	10
$i_{v,d}$	0.5	0.5	0	0	0	0	0	0	0	0
$i_{v,q}$	0.5	0.5	0	0	0	0	0	0	0	0
$v_{f,d}$	0	0	0.2476	0.2476	0.2524	0.2524	0	0	0	0
$v_{f,q}$	0	0	0.2524	0.2524	0.2476	0.2476	0	0	0	0
$i_{g,d}$	0	0	0.2476	0.2476	0.2524	0.2524	0	0	0	0
$i_{g,q}$	0	0	0.2521	0.2521	0.2471	0.2471	0	0	0.0044	0.0044
δ	0	0	0.0004	0.0004	0.0004	0.0004	0	0	0.4976	0.4976
A	0	0	0	0	0	0	0.5	0.5	0	0
B	0	0	0	0	0	0	0	0	0.498	0.498
C	0	0	0	0	0	0	0.5	0.5	0	0

E.2 Alternative 0

Table E.3: The eigenvalues of the alternative 0 model when δ is estimated.

Eigenvalue Nr.	Real	Imaginary
1	-6.41E+07	+ 201.92i
2	-6.41E+07	- 201.92i
3	-85.405	+ 7769.4i
4	-85.405	- 7769.4i
5	-81.044	+ 7141.1i
6	-81.044	- 7141.1i
7	-650.01	+ 0i
8	-650	+ 0i
9	-0.28484	+ 2.0961i
10	-0.28484	- 2.0961i

Table E.4: The participation factors related to the eigenvalues in Table E.3.

	Eigenvalue Number									
	1	2	3	4	5	6	7	8	9	10
$i_{v,d}$	0.5	0.5	0	0	0	0	0	0	0	0
$i_{v,q}$	0.5	0.5	0	0	0	0	0	0	0	0
$v_{f,d}$	0	0	0.2483	0.2483	0.2517	0.2517	0	0	0	0
$v_{f,q}$	0	0	0.2517	0.2517	0.2482	0.2482	0	0	0	0
$i_{g,d}$	0	0	0.2483	0.2483	0.2517	0.2517	0	0	0	0
$i_{g,q}$	0	0	0.2514	0.2514	0.2479	0.2479	0	0	0.0022	0.0022
δ	0	0	0.0004	0.0004	0.0004	0.0004	0	0	0.4988	0.4988
A	0	0	0	0	0	0	0.8822	0.1178	0	0
B	0	0	0	0	0	0	0	0	0.499	0.499
C	0	0	0	0	0	0	0.1178	0.8822	0	0

E.3 Alternative 1

Table E.5: The eigenvalues of the alternative 1 model when δ is estimated.

Eigenvalue Nr.	Real	Imaginary
1	-6.41E+07	+ 311.92i
2	-6.41E+07	- 311.92i
3	-195.98	+ 7436.6i
4	-195.98	- 7436.6i
5	-927.34	+ 7572.7i
6	-927.34	- 7572.7i
7	941.45	+ 0i
8	-130	+ 0.00040292i
9	-130	- 0.00040292i
10	-7.9192	+ 0i

Table E.6: The participation factors related to the eigenvalues in Table E.5

	Eigenvalue Number									
	1	2	3	4	5	6	7	8	9	10
$i_{v,d}$	0.5	0.5	0	0	0	0	0	0	0	0
$i_{v,q}$	0.5	0.5	0	0	0	0	0	0	0	0
$v_{f,d}$	0	0	0.4383	0.4383	0.0567	0.0567	0.0001	0	0	0
$v_{f,q}$	0	0	0.0579	0.0579	0.4199	0.4199	0.017	0	0	0
$i_{g,d}$	0	0	0.4392	0.4392	0.0574	0.0574	0	0	0	0
$i_{g,q}$	0	0	0.057	0.057	0.4135	0.4135	0.0378	0	0	0
δ	0	0	0.0076	0.0076	0.0524	0.0524	0.9374	0	0	0.008
A	0	0	0	0	0	0	0	0.5	0.5	0
B	0	0	0	0	0.0001	0.0001	0.0077	0	0	0.992
C	0	0	0	0	0	0	0	0.5	0.5	0

E.4 Alternative 2

Table E.7: The eigenvalues of the alternative 2 model when δ is estimated.

Eigenvalue Nr.	Real	Imaginary
1	-6.41E+07	+ 312.79i
2	-6.41E+07	- 312.79i
3	-82.523	+ 7459.5i
4	-82.523	- 7459.5i
5	-8548.8	+ 0i
6	6416.2	+ 0i
7	991.1	+ 0i
8	-130	+ 0.00032798i
9	-130	- 0.00032798i
10	-7.9189	+ 0i

Table E.8: The participation factors related to the eigenvalues in Table E.7

	Eigenvalue Number									
	1	2	3	4	5	6	7	8	9	10
$i_{v,d}$	0.5	0.5	0	0	0	0	0	0	0	0
$i_{v,q}$	0.5	0.5	0	0	0	0	0	0	0	0
$v_{f,d}$	0	0	0.4999	0.4999	0.0001	0.0001	0.0001	0	0	0
$v_{f,q}$	0	0	0.0001	0.0001	0.4977	0.4298	0.0098	0	0	0
$i_{g,d}$	0	0	0.4999	0.4999	0.0001	0.0001	0.0001	0	0	0
$i_{g,q}$	0	0	0.0001	0.0001	0.4537	0.489	0.0342	0	0	0
δ	0	0	0.0001	0.0001	0.0484	0.0808	0.9483	0	0	0.008
A	0	0	0	0	0	0	0	0.5	0.5	0
B	0	0	0	0	0.0001	0.0002	0.0076	0	0	0.992
C	0	0	0	0	0	0	0	0.5	0.5	0

Appendix F

Eigenvalues and Participation factor when δ is removed. Alternative 1

Table F.1: Eigenvalues without the δ term. Alt1

Eigenvalue Nr.	Real	Imaginary
1	-6.41E+07	+ 312.27i
2	-6.41E+07	- 312.27i
3	-175.01	+ 7439.5i
4	-175.01	- 7439.5i
5	-1116.4	+ 7598.7i
6	-1116.4	- 7598.7i
7	1097.6	+ 0i
8	-130	+ 0.00048418i
9	-130	- 0.00048418i
10	-7.929	+ 0i

Table F.2: Participation factor without the δ term. Alt 1

	Eigenvalue Number									
	1	2	3	4	5	6	7	8	9	10
$i_{v,d}$	0.5	0.5	0	0	0	0	0	0	0	0
$i_{v,q}$	0.5	0.5	0	0	0	0	0	0	0	0
$v_{f,d}$	0	0	0.4568	0.4568	0.039	0.039	0.0001	0	0	0
$v_{f,q}$	0	0	0.04	0.04	0.4333	0.4333	0.022	0	0	0
$i_{g,d}$	0	0	0.4577	0.4577	0.0398	0.0398	0	0	0	0
$i_{g,q}$	0	0	0.0392	0.0392	0.4249	0.4249	0.0488	0	0	0
δ	0	0	0.0063	0.0063	0.0628	0.0628	0.9226	0	0	0.0068
A	0	0	0	0	0	0	0	0.5	0.5	0
B	0	0	0	0	0.0001	0.0001	0.0065	0	0	0.9932
C	0	0	0	0	0	0	0	0.5	0.5	0

Appendix G

Steady State Calculations, Alt1 Script

```
function F = alt_1_try(x,kp_cc,ki_cc,kp_pll,ki_pll,ivd_ref,ivq_ref,tau,vgd,vgq,vdc,↙
delta_ref,lf,lg,c,rf,rg,wg)
delta_real=x(7);
delta_estimate=atan2(x(4),x(3));

y_1=vdc*(x(1)-ivd_ref);
y_2=lf*(x(1)*ivq_ref-x(2)*ivd_ref)+c*(x(3)*x(4)-x(4)*x(3))+tau*(delta_real-↙
delta_ref);
y_3=vdc*(x(2)-ivq_ref);

ed=-kp_cc*y_1+ki_cc*x(8);
eq=-kp_cc*y_3+ki_cc*x(10);

w_pll=-kp_pll*y_2+ki_pll*x(9);


F(1)=(ed-rf*x(1)+w_pll*(lf*x(2))-x(3))/lf; %ivd
F(2)=(eq-w_pll*(lf*x(1))-rf*x(2)-x(4))/lf; %ivq

F(3)=(w_pll*(c*x(4))+x(1)-cos(delta_real)*x(5)+sin(delta_real)*x(6))/c; %v0d
F(4)=(-w_pll*(c*x(3))+x(2)-sin(delta_real)*x(5)-cos(delta_real)*x(6))/c; %v0q

F(5)=(cos(delta_real)*x(3)+sin(delta_real)*x(4)-rg*x(5)+lg*wg*x(6)-vgd)/lg; %igd
F(6)=(-sin(delta_real)*x(3)+cos(delta_real)*x(4)-lg*wg*x(5)-rg*x(6)-vgq)/lg; %igq

F(7)=w_pll-wg; %delta

F(8)=-y_1; %A
F(9)=-y_2; %B
F(10)=-y_3; %C

end
```

```
format short
clear
clc
% %LCL filter
lf=3.82e-3;
rf=0.05; %0.05
lg=300e-6;
c=60e-6;
rg=0.05;
vac=400;
% %CC
 kp_cc=0.5*700;
 ki_cc=65*700;

% %Grid
wg=2*pi*50; %Hz
vgd=(sqrt(2)*vac)/sqrt(3);
vgq=0;
vdc=700;
% %PLL
 kp_pll = 180;
 ki_pll = 1437;
 tau=1;

%steady state

ivd_ref=10;
ivq_ref=0;
delta_ref=0;



fun= @ (x)alt_1_try(x,kp_cc,ki_cc,kp_pll,ki_pll,ivd_ref,ivq_ref,tau,vgd,vgq,vdc,↙
delta_ref,lf,lg,c,rf,rg,wg);
x0=[10;0;300;0;0;0;0;0;0;0];
X=fsolve(fun,x0)

ivd_0=X(1);
ivq_0=X(2);
v0d_0=X(3);
v0q_0=X(4);
igd_0=X(5);
igq_0=X(6);
delta_0=X(7);
A_0=X(8);
B_0=X(9);
C_0=X(10);
```

Appendix H

Stability Calculations, Alt 1 Script

```
format short g

syms lf rf lg c rg   %LCL
syms kp_cc ki_cc  %CC
syms kp_pll ki_pll tau % PLL
syms wg vgd vgq vdc %grid
syms ivd_ref ivq_ref delta_ref v0d_ref v0q_ref %Steady state
syms ivd ivq v0d v0q igd igq delta A B C %States +virtual states

%% Simulink model
vac=400;%v
fsw=10e+3; %Switch. freq
fsamp=10e+3; %sampling time
Tf=0.0005;

%% Real values
lf_0=3.82e-3;
rf_0=0.05;
c_0=60e-6;
rg_0=0.05;
lg_0=300e-6;
%CC
 kp_cc_0=0.5*700;
 ki_cc_0=65*700;

%Grid
wg_0=2*pi*50; %Hz
vgd_0=(sqrt(2)*vac)/sqrt(3);
vgq_0=0;
vdc_0=700;


%PLL
kp_pll_0 = 180;
ki_pll_0 = 1437;
tau_0=1;

%% Jacobian
delta_real=delta;
delta_est=atan2(v0q,v0d);

y_1=vdc*(ivd-ivd_ref);
y_2=lf*(ivd*ivq_ref-ivq*ivd_ref)+c*(v0d*v0q_0-v0q*v0d_0)+tau*(delta_real-delta_ref);
y_3=vdc*(ivq-ivq_ref);

ed=-kp_cc*y_1+ki_cc*A;
eq=-kp_cc*y_3+ki_cc*C;

w_pll=-kp_pll*y_2+ki_pll*B;

d_ivd=(ed-rf*ivd+w_pll*(lf*ivq)-v0d)/lf;
d_ivq=(eq-w_pll*(lf*ivd)-rf*ivq-v0q)/lf;

d_v0d=(w_pll*(c*v0q)+ivd-cos(delta_real)*igd+sin(delta_real)*igq)/c;
```

```
d_v0q=(-w_pll*v0d*c+ivq-sin(delta_real)*igd-cos(delta_real)*igq)/c;

d_igd=(cos(delta_real)*v0d+sin(delta_real)*v0q-rg*igd+lg*wg*igq-vgd)/lg;
d_igq=(-sin(delta_real)*v0d+cos(delta_real)*v0q-lg*wg*igd-rg*igq-vgq)/lg;

d_delta=w_pll-wg;
d_A=-y_1;
d_B=-y_2;
d_C=-y_3;

f=[d_ivd,d_ivq,d_v0d,d_v0q,d_igd,d_igq,d_delta,d_A,d_B,d_C];
x=[ivd,ivq,v0d,v0q,igd,igq,delta,A,B,C] ;
u=[ivd_ref,ivq_ref,delta_ref];

Jac_A = jacobian(f,x); %Calculate the A matrix algebraic
Jac_B = jacobian (f,u); %Calculate the B matrix algebraic


ivd_ref_0=ivd_0;
ivq_ref_0=ivq_0;
delta_ref_0=delta_0;
v0d_ref_1=v0d_0;
v0q_ref_1=v0q_0;

%Substitute the algebraic components of the A and B matrix with values.
Aaaa=subs(Jac_A,[ivd,ivq,v0d,v0q,igd,igq,delta,A,B,C,ivd_ref,ivq_ref,delta_ref,↙
kp_cc,kp_pll,ki_cc,ki_pll,lf,rf,c,lg,rg,wg,vgd,vgq,vdc,tau,v0d_ref,v0q_ref]...
    ,[ivd_0,ivq_0,v0d_0,v0q_0,igd_0,igq_0,delta_0,A_0,B_0,C_0,ivd_ref_0,ivq_ref_0,↙
delta_ref_0,kp_cc_0,kp_pll_0,ki_cc_0,ki_pll_0,lf_0,rf_0,c_0,lg_0,rg_0,wg_0,vgd_0,↙
vgq_0,vdc_0,tau_0,v0d_ref_1,v0q_ref_1]); %Bytte ut bokstaver med værdier
Bbbb=subs(Jac_B,[ivd,ivq,v0d,v0q,igd,igq,delta,A,B,C,ivd_ref,ivq_ref,delta_ref,↙
kp_cc,kp_pll,ki_cc,ki_pll,lf,rf,c,lg,rg,wg,vgd,vgq,vdc,tau,v0d_ref,v0q_ref],...
[ivd_0,ivq_0,v0d_0,v0q_0,igd_0,igq_0,delta_0,A_0,B_0,C_0,ivd_ref_0,ivq_ref_0,↙
delta_ref_0,kp_cc_0,kp_pll_0,ki_cc_0,ki_pll_0,lf_0,rf_0,c_0,lg_0,rg_0,wg_0,vgd_0,↙
vgq_0,vdc_0,tau_0,v0d_ref_1,v0q_ref_1]);

A_mat=double(Aaaa);
B_mat=double(Bbbb);
C_mat=[1,0,0,0,0,0,0,0,0,0;0,1,0,0,0,0,0,0,0,0;0,0,1,0,0,0,0,0,0,0;↙
0,0,0,1,0,0,0,0,0,0;0,0,0,0,1,0,0,0,0,0;0,0,0,0,0,1,0,0,0,0;0,0,0,0,0,0,1,0,0,0;↙
0,0,0,0,0,0,0,1,0,0;0,0,0,0,0,0,0,0,1,0;0,0,0,0,0,0,0,0,0,1]';
D_mat=[0,0,0,0,0,0,0,0,0,0;0,0,0,0,0,0,0,0,0,0;0,0,0,0,0,0,0,0,0,0]';

% Participation factor
[V,D]=eig(A_mat);
V; %Right eigenvector
W=inv(V); %Left eigenvectors
Eigen=eig(A_mat);

%% Participation factor
for i=1:10
    for k=1:10
    P(k,i)=abs(V(k,i)*W(i,k));
    k=k+1;
```

```
    end
    i=i+1;
end

% In order to get the sum of each eigenvalue to 1
for j=1:10
    for g=1:10
        G(g,j)=P(g,j)/sum(P(:,j));
        g=g+1;
    end
    j=j+1;
end

%% For the plotting of the eigenvalues as well as changing parameters to track the↙
different eigenvalues.

% %% Plot Eigenvalue
% figure; hold on
% %lg_0=0 %linspace(350e-10,100e-7,6);
% for tau_0=1 %Possibility to chane the parameter in order to trach the change of↙
the different eigenvalues
% Aaa=subs(Jac_A,[ivd,ivq,v0d,v0q,igd,igq,delta,A,B,C,ivd_ref,ivq_ref,delta_ref,↙
kp_cc,kp_pll,ki_cc,ki_pll,lf,rf,c,lg,rg,wg,vgd,vgq,vdc,tau]...
%     ,[ivd_0,ivq_0,v0d_0,v0q_0,igd_0,igq_0,delta_0,A_0,B_0,C_0,ivd_ref_0,ivq_ref_0,↙
delta_ref_0,kp_cc_0,kp_pll_0,ki_cc_0,ki_pll_0,lf_0,rf_0,c_0,lg_0,rg_0,wg_0,vgd_0,↙
vgq_0,vdc_0,tau_0]);
% A_matrix=double(Aaa);
% GR=eig(A_matrix);
% plot(GR,'*');
% xlabel('Real')
% ylabel('Imaginary')
% end
%
%
% %% Participation factor
% [V,D]=eig(A_matrix);
% V; %Right eigenvector
% W=inv(V); %Left eigenvectors
% Eigen=eig(A_matrix);
% %% Participation factor
% for i=1:10
%     for k=1:10
%     P(k,i)=abs(V(k,i)*W(i,k));
%     k=k+1;
%     end
%     i=i+1;
% end
%
% % In order to get the sum of each eigenvalue to 1
% for j=1:10
%     for g=1:10
%         G(g,j)=P(g,j)/sum(P(:,j));
%         g=g+1;
%     end
```

```
%     j=j+1;
% end
```

Rune Steig

Towards Energy Synchronization of Two-Level Voltage Source Converters

NTNU
Norwegian University of
Science and Technology